Investigation of Sensitivity of Surface Deformation to Subsurface Properties and Reservoir Operations

by
Pui-Wa Li

B.S. Civil and Environmental Engineering
University of California, Berkeley, 2010

SUBMITTED TO THE DEPARTMENT OF CIVIL AND EVIRONMENTAL ENGINEERING
FULFILLMENT OF THE REQUIREMENTS FOR THE DEGREE OF

MASTER OF SCIENCE IN CIVIL AND ENVIRONMENTAL ENGINEERING
AT THE
MASSACHUSETTS INSTITUTE OF TECHNOLOGY

JUNE 2012

Signature of Author: _____
Department of Civil and Environmental Engineering
May 29, 2012

Certified by: _____
Dennis B. McLaughlin
H.M. King Bhumibol Professor of Civil and Environmental Engieering
Thesis Supervisor

Accepted by: _____
Heidi M. Nepf
Chair, Departmental Committee for Graduate Students

Investigation of Sensitivity of Surface Deformation to Subsurface Properties and Reservoir Operations

by

Pui-Wa Li

Submitted to the Department of Civil and Environmental Engineering
on May 29, 2012 in Partial Fulfillment of the
Requirements for the Degree of Master of Science in
Civil and Environmental Engineering

ABSTRACT

An experimental study is performed to understand the sensitivity of ground deformation to subsurface properties and operations of oil and gas fields. Ground deformation, or more severely subsidence, may pose concerns for human settlements situated above the reservoir. This Masters thesis will study a realistic sample problem on its surface deformation sensitivity, in hopes of providing a sound basis for future characterization of subsurface properties and the forecast of surface deformation due to oil and gas production.

Iteratively coupled simulations are performed to test how sensitive the surface deformation is to changing subsurface parameters. To test the validity of such coupled simulator, comparison of the displacement results with those of another commercially available software is also carried out. Results show that the change of surface displacement particularly in the vertical direction tends to be within the range of detection of satellites, of which data will serve as the input of future inversions with the Ensemble Kalman Filter (EnKF).

Thesis Supervisor: Dennis B. McLaughlin
Title: H.M. King Bhumibol Professor of Civil and Environmental Engineering

Table of Contents

Acknowledgement

I would like to express my thanks to ENI. ENI has funded my Masters study through its ENI's "Multiscale Reservoir Science for Enhanced Oil Recovery: Technology Development and Field Applications" within the MIT-Energy Initiative Founding Member Program. Being part of this cross-campus, interdepartmental research collaborative effort, I was able to learn many things both within and outside my field of study in Hydrology. This project allowed me to make fruitful collaborative efforts with ENI's personnel, including Alberto Cominelli and Francesca Bottazzi. Francesca, in particularly, has given me a lot of support on this work which I really appreciate, gave her experience in the industry.

Because of this project, I was very lucky to work with Professor Brad Hager from the Earth, Astompheric, and Planetary Science Department. Brad taught me in his class Geodynamics. He has given me countless advice on geomechanics modeling. Without his help, I would not be able to attain this much. I would like to express gratitude to Professor Tom Herring and Professor Ruben Juanes. Tom not only let me to work with his student Martina but also gave a helping hand by resolving the cluster issue at the most critical moment. Without his help, I would not be able to finish all the simulation runs in a timely manner. With Ruben, I was able to learn a lot from his class Computational Methods for Flow in Porous Media. I appreciate very much his time in giving advice to my research, along with the help of his student Birendra Jha.

By taking classes in mechanics, I was able to meet students from other departments. Not to mention the good time studying with Stephane Marcadet and Aalap Dighe; they both offered massive help in any circumstances, mechanics in particular, and introduced me to so many people. Special thanks to Jean-Philippe Péraud for the selfless support and countless encouragement. Special thanks to Martina Coccia for her wonderful jokes, support, understanding advice and Italian recipes; Sedar Sahin for his encouragement and generosity; Lukas Willaimsen for the good conversation and the negative victory points in Dominion; Haoyue Wang for his shrewdness and great help; and all the students from the Geodynamics class. They all have offered me a lot of help and support throughout this research project in many different ways.

Special thanks to Binghuai, who has given me huge support from the beginning till the end. It was one of my biggest pleasures to discover our common sub-cultural background that was almost lost with the huge difference in the linguistic accent. Now I know that Hakka dialect would no longer be my secret code at MIT.

Last but not least, I would like to express the deepest thanks to Professor Dennis McLaughlin. Dennis has given me invaluable advice and support throughout the project. It is always wonderful to consult Dennis on any occasion. I really appreciate the time he has put and invested in my intellectual growth. His jokes have always brightened up our days, changing pressure to pleasure at MIT. Without his advice and the directions he gave, I would not be able to meet and work with all the professors, friends and students whom I have mentioned above.

Chapter 1 - Introduction

Motivation

Surface subsidence due to oil and gas production can pose substantial implications to the human settlements situated on the ground surface above the reservoir. A good understanding of the sensitivity of ground deformation to the subsurface properties and operations of oil and gas fields would be helpful in utilizing surface deflection data observed by the interferometric synthetic aperture radar (INSAR) to estimate properties of the reservoir. This Masters thesis will simulate a realistic sample problem and analyze such sensitivity, in hopes of providing a sound basis for future characterization of subsurface properties and the forecast of surface deformation due to oil and gas production.

Objective

We are interested in testing the coupled flow and geomechanics models on a realistic sample problem, a black-oil model operated by Elf Exploration Production (to be further described in Chapter 4 –Sample Problem (PUNQ)). This is done by first comparing the results of pressure field and displacement fields simulated by commercially available software through one-way coupling of fluid flow and geomechanics. Using a forward model called CMG STARS, we will explore the surface deformation computed as a result of iterative coupling. Then we will find out the sensitivity of ground deformation due to various subsurface properties of PUNQ.

Background and Literature Review

We hope to apply principles that can help us better calculate deformations in general. It is known by Terzaghi (Terzaghi) that deformation of the soil is due to changes in the effective stress, after taking into account of the pore pressure which counteracts the load of the total stress applied on the soil. But during oil and gas production, pore pressure changes through time (and subsequently the effective stress too) and that time-dependent change shall be taken into account for computational purposes. Also, Geertsma (Geertsma) realized that changes in pore pressure can alter the size of the pore space. These call for the need of a forward model that truly couples fluid flow and geomechanics.

As one of the next steps, we would like to estimate subsurface properties and surface deformation using Ensemble Kalman Filter (EnKF) in the near future. Previous efforts demonstrated the usefulness of EnKF. Both Chen (Chang, Chen and Zhang)and Vasco (Vasco)

did inversions on coupled fluid flow and geomechanics. Through coupled inversion, Vasco et al. characterized the permeability field of the reservoir based on pressure changes in boreholes and surface deflection data. Chen et al. used EnKF to estimate reservoir flow, permeability and Young's modulus based on known production observations (such as the production schedule, well bottom-hole pressure and water cuts) and surface deformation data.

Theoretical Background

To understand the sensitivity of surface deformation to subsurface properties of an oil reservoir, we need to understand the formulation of the fluid flow and geomechanics constitutive equations. In general, fluid flow due to oil production can reduce pore pressure within the reservoir. If so, this can drive the ground surface to go downward. Injection into the reservoir, on the other hand, increases pore pressure and the ground might bulge depending on the increase of pore pressure. During computation, how much interaction is allowed between the two constitutive equations [Equations 4 to 6 and Equation 8] in fact plays an important role in seeking an acceptable solution without compromising accuracy, adaptability, and simulation speed (Tran, Nghiem and Buchanan).

Chapter 2 – Governing Equations

Fluid Flow Equations

Single-Component, Single-Phase Flow System

The material balance equation, Darcy's law, and energy conservation govern the fluid flow in porous medium. Since the problem of our interest is in isothermal mode, there is no need to apply the equation of energy conservation here. Combining Darcy's law and material balance, mass conservation is described by:

$$\frac{\partial}{\partial t}(\theta^* \rho_f) - \nabla \cdot \left(\rho_f \frac{\boldsymbol{K}}{\mu} \cdot [\nabla p - \rho_f \boldsymbol{b}]\right) = Q_f$$

Equation 1

where $\theta^* = \frac{current\ pore\ volume}{initial\ bulk\ volume}$ or the reservoir porosity [unitless], $\boldsymbol{K}$ is the tensor for absolute permeability [md], μ is the dynamic viscosity of fluid, ∇p is the pore pressure gradient in the field $[kPa]$, $\boldsymbol{b}$ is the body force per unit mass acting on the fluid $[m/s^2]$, ρ_f is the fluid density $[\frac{kg}{m^3}]$, and Q_f is the fluid flow rate (due to production or injection)$[\frac{kg}{m^3}]$.

Please note that this equation only applies to single-component, single-phase flow systems (Tran, Nghiem and Buchanan).

Multiphase Fluid Flow in a Black-Oil Model

As we are dealing with a black-oil model, however, there are oleic, gaseous and aqueous phases. Among these phases, the water and oil component always stays in the same phase while the gas component can switch between oleic phase and gaseous phase. For example, hydrocarbons like methane or ethane may exist in both oleic and gaseous forms, transferring mass from one phase to another.

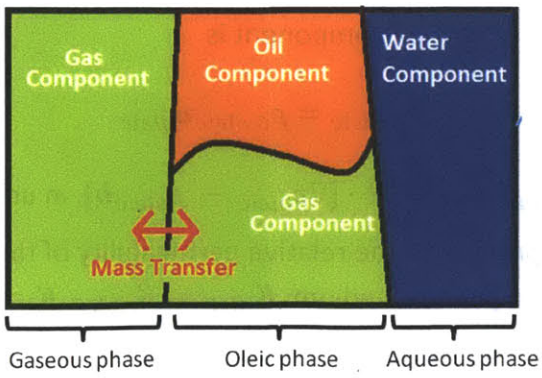

Figure 1 Saturation of phases in a black-oil model. Note the mass transfer of gas component in between gaseous and oleic phases.

Figure 1 illustrates the idea of mass transfer between phases. Within the void space, there can be only three phases. The three saturations, being unitless, together add up to $S_{aqueous} + S_{oleic} + S_{gaseous} = 1$.

Given mass transfer between phases, we cannot ensure that mass is conserved within each phase at all time. Therefore a material balance on each component is more suitable here. The capital letter subscripts O, G, W represent the oil, gas and water components, respectively.

For the oil component,

$$\frac{\partial m_{O,oleic}}{\partial t} + \nabla \cdot \boldsymbol{F_{O,oleic}} = q_O$$

Equation 2

where q_O is the flow rate of the oil component $[\frac{m^3}{s}]$ at the source and sink location.

The mass concentration of the oil component in oleic phase ($m_{O,oleic}$ $[kg]$) is

$$m_{O,oleic} = \frac{M_{O,oleic}}{V_{porous\ medium}} = \left(\frac{M_{O,oleic}}{V_{oleic}}\right)\left(\frac{V_{oleic}}{V_{void}}\right)\left(\frac{V_{void}}{V_{porous\ medium}}\right) = \rho_{O,oleic} S_{oleic} \theta$$

Equation 3

where $\rho_{O,oleic}$ is the partial density of the oil component in oleic phase $[\frac{kg}{m^3}]$ with $\rho_{oleic} = \rho_{O,oleic} + \rho_{G,oleic}$(summing up the components in one phase). S_{oleic} is the oleic phase saturation $[unitless]$.

The mass flux $\boldsymbol{F_{O,oleic}}$ $\left[\frac{\boldsymbol{kg}}{\boldsymbol{m^2 \cdot s}}\right]$of the oil component is

$$\boldsymbol{F_{O,oleic}} = \rho_{O,oleic} \boldsymbol{u_{oleic}}$$

given that the velocity $\boldsymbol{u_{oleic}} = -\frac{\boldsymbol{K_{oleic}}}{\mu} \cdot [\nabla p_{oleic} - \rho_{oleic} \boldsymbol{b}]$, in unit of $\frac{m}{s}$, and that the phase permeability is the product of the relative permeability of the oleic phase and the absolute permeability of the porous medium, $\boldsymbol{K_{oleic}} = K_{r,oleic} \boldsymbol{K} = [md] = [unitless] \cdot [md]$.

The material balance equation for oil component now becomes

$$\frac{\partial \rho_{O,oleic} S_{oleic} \theta}{\partial t} - \nabla \cdot \left(\rho_{O,oleic} \frac{\boldsymbol{K_{oleic}}}{\mu} \cdot [\nabla p_{oleic} - \rho_{oleic} \boldsymbol{b}] \right) = q_O$$

Equation 4

As the gas component exist in both gaseous and oleic phases,

$$\frac{\partial (\rho_{G,oleic} S_{oleic} + \rho_{gaseous} S_{gaseous}) \theta}{\partial t} - \nabla \cdot (\rho_{G,oleic} \boldsymbol{u_{oleic}} + \rho_{gaseous} \boldsymbol{u_{gaseous}}) = q_G$$

$$\frac{\partial (\rho_{G,oleic} S_{oleic} + \rho_{gaseous} S_{gaseous}) \theta}{\partial t} - \nabla \cdot \left(\rho_{G,oleic} \frac{\boldsymbol{K_{oleic}}}{\mu} \cdot [\nabla p_{oleic} - \rho_{oleic} \boldsymbol{b}] + \rho_{gaseous} \frac{\boldsymbol{K_{gaseous}}}{\mu} \cdot [\nabla p_{gaseous} - \rho_{gaseous} \boldsymbol{b}] \right) = q_G$$

Equation 5

And lastly, for the water component, which only exists in aqueous phase,

$$\frac{\partial \rho_{aqueous} S_{aqueous} \theta}{\partial t} - \nabla \cdot \left(\rho_{aqueous} \frac{\boldsymbol{K_{aqueous}}}{\mu} \cdot [\nabla p_{aqueous} - \rho_{aqueous} \boldsymbol{b}] \right) = q_W$$

Equation 6

(Chen, Huan and Ma).

Geomechanics Equation

In general, the deformation of the ground can be described by the force balance equation

$$\nabla \cdot \left[\mathbf{C} : \frac{1}{2} (\nabla \mathbf{u} + (\nabla \mathbf{u})^T) \right] = \rho_r \mathbf{b} - \nabla \cdot [(\alpha p - \eta \Delta T) \boldsymbol{I}]$$

Equation 7

which relates the pore pressure gradient ∇p to the deformation of the medium $[kPa]$, and ∇p would only apply to the porous zone. Since our system here is isothermal, the equation is simplified to

$$\nabla \cdot \left[\mathbf{C} : \frac{1}{2} (\nabla \mathbf{u} + (\nabla \mathbf{u})^T) \right] = \rho_r \mathbf{b} - \nabla \cdot [\alpha p \boldsymbol{I}]$$

Equation 8

where strain is $\boldsymbol{\epsilon} = \frac{1}{2}(\nabla \mathbf{u} + (\nabla \mathbf{u})^T)$and is unitless,

effective stress is $\boldsymbol{\sigma_{eff}} = \boldsymbol{C} : \boldsymbol{\epsilon} - \eta \Delta T \boldsymbol{I} = \boldsymbol{C} : \boldsymbol{\epsilon}$ and has the unit of kPa,

total stress is $\boldsymbol{\sigma} = \boldsymbol{\sigma_{eff}} - \alpha p \boldsymbol{I}$ has the unit of kPa,,

and $\mathbf{u}$ = displacement vector $[m]$, $\boldsymbol{C}$ = stiffness tensor $[kPa]$, ρ_r = rock density $[\frac{kg}{m^3}]$, $\mathbf{b}$ = body force per unit mass acted on the rock $\left[\frac{m}{s^2}\right]$, α = Biot's constant $[unitless]$ (Tran, Nghiem and Buchanan).

Since the material in our simulation is isotropic,

$$\boldsymbol{C} = c_{ijkl} = \lambda \delta_{ij} \delta_{kl} + \mu(\delta_{ik}\delta_{jl} + \delta_{il}\delta_{jk})$$

Equation 9

with Lamé parameters λ and μ, with units of kPa. Thus,

$$\boldsymbol{\sigma_{eff}} = \sigma_{eff,ij} = \lambda \epsilon_{kk} \delta_{ij} + 2\mu \epsilon_{ij}$$

Equation 10

Boundary and Initial Conditions for Base Case

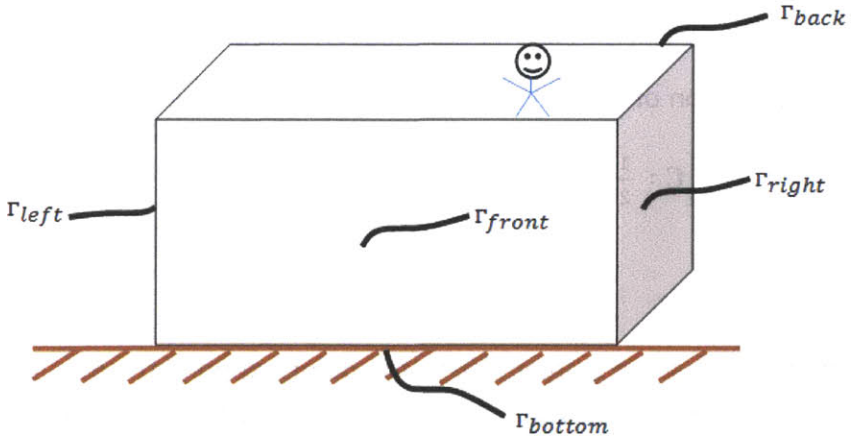

Figure 2 A 3D-viewof the geomechanics grid

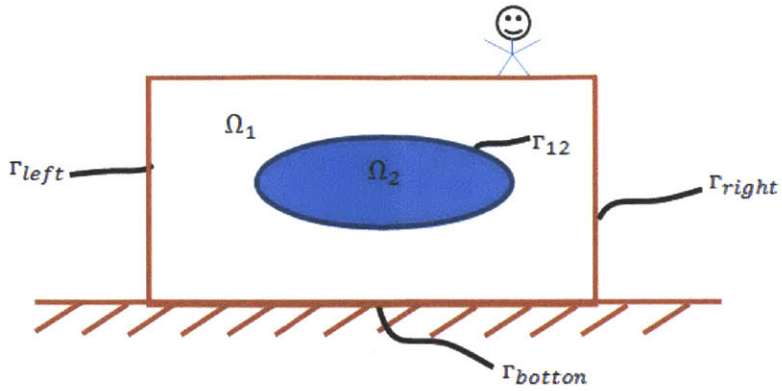

Figure 3 A simplified cross-sectional view of the geomechanics grid

For the geomechanics grid Ω_1, the following boundary conditions are prescribed:

$$\mathbf{u} = \mathbf{0}\ at\ the\ four\ corners\ on\ _{bottom}\ and\ \mathbf{u} = \begin{bmatrix} \mathbf{u_x} \\ \mathbf{u_y} \\ \mathbf{0} \end{bmatrix} elsewhere\ on\ _{bottom}$$

$$\mathbf{u} \cdot \hat{\mathbf{n}} = 0\ and\ \hat{\boldsymbol{n}} \cdot \boldsymbol{\sigma}\widehat{\boldsymbol{e_z}} = 0\ on\ _{left\,,right,front}\ and\ _{back}$$

$$with\ \widehat{\boldsymbol{e_x}} \cdot \boldsymbol{\sigma}\widehat{\boldsymbol{e_y}} = 0\ and\ \widehat{\boldsymbol{e_x}} \cdot \boldsymbol{\sigma}\widehat{\boldsymbol{e_z}} = 0\ on\ _{left\,,right}$$

$$\widehat{\boldsymbol{e_x}} \cdot \boldsymbol{\sigma}\widehat{\boldsymbol{e_y}} = 0\ and\ \widehat{\boldsymbol{e_y}} \cdot \boldsymbol{\sigma}\widehat{\boldsymbol{e_z}} = 0\ on\ _{front\,,back}$$

Equation 11

For the flow grid Ω_2, the following boundary condition is applied:

$$\mathbf{u} \cdot \boldsymbol{n} = \mathbf{0}$$

Equation 12

Across the interface $_{12}$, the no-flow condition is applied(no change of pressure normal to the interface) is prescribed:

$$\nabla \boldsymbol{p} \cdot \hat{\boldsymbol{n}} = 0$$

Equation 13

The initial conditions are

$$p(t = 0) = p_0 \, in \, \Omega_2,$$

$$\mathbf{u}(t = 0) = \mathbf{0} \; in \, \Omega_1 \cup \Omega_2,$$

Equation 14

Boundary Conditions for Abaqus and STARS Displacement Comparison

For comparing the displacement field of STARS and Abaqus in Chapter 5 –Model Comparison Result, we use another set of boundary conditions. They are as follow:

$$\mathbf{u} = \mathbf{0} \; on_{\; bottom}$$

$$\mathbf{u} = \mathbf{0} \; on_{left \, , \, right \, , \, front} \; and_{\; back}$$

Equation 15

Chapter 3 – Experimental Procedure

We will carry out several tests comparing the results of different forward models. After that, sensitivity analyses will be done on the sample problem, in order to understand the link between subsurface properties and surface deformation. The flowchart of the experimental procedure is summarized below in Figure 4.

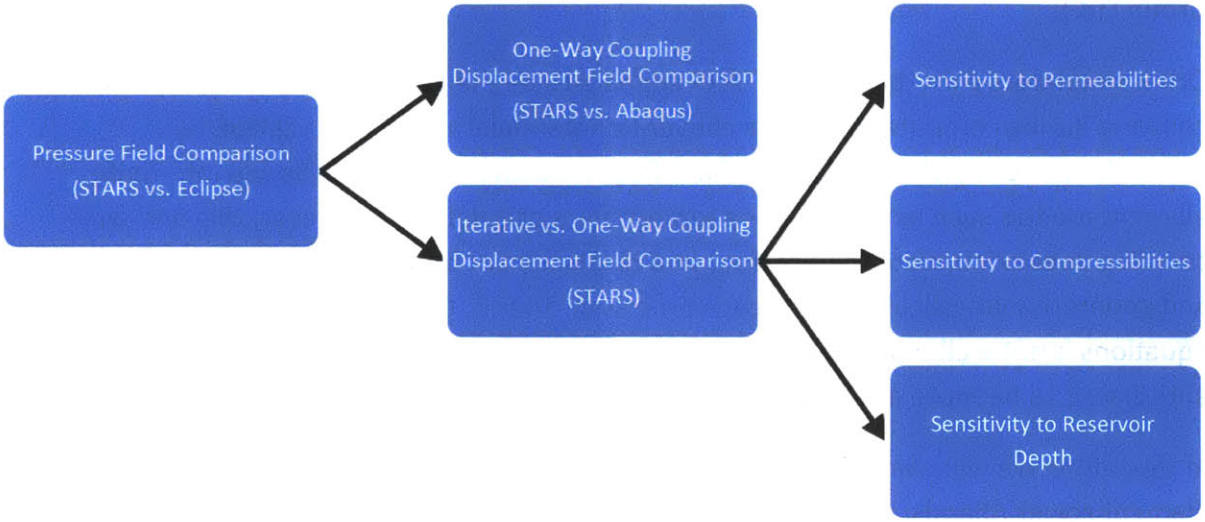

Figure 4 Summary of the tests being done during this study

Models Studied (STARS vs. Eclipse/Abaqus)

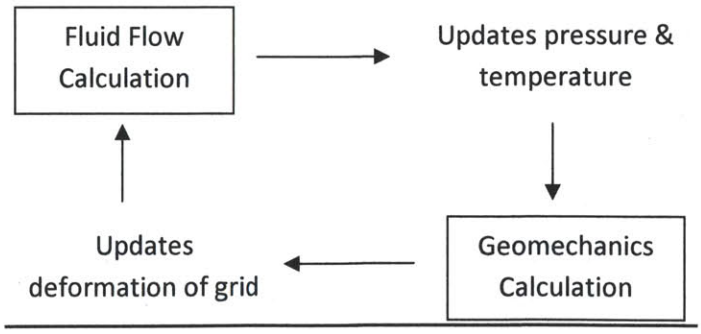

Figure 5: Schematics of coupled calculation of fluid flow and geomechanics

The model of interest is the Steam, Thermal, and Advanced Processes Reservoir Simulator (STARS) developed by the Computer Modeling Group in Calgary, Canada. STARS is a thermal

compositional simulator. It features calculation by iteratively coupling geomechanics to fluid flow, where porosity is a function of pressure and temperature. At time t, the fluid flow module calculates the formation pressures and temperature, which are then passed on to the geomechanics module. Due to this change of pressure and temperature, the deformation of the formation is calculated and is then passed back to the fluid flow module. This closes the iterative coupling loop for the next round of calculation at time $t+\Delta t$. During each time interval, the fluid and formation masses are conserved (Computer Modeling Group Ltd.).

Other simulators exist, but so far STARS appears to be the simulator which incorporates true coupling during computation. More conventional simulators such as ECLIPSE by Schlumberger can yield the result of fluid-flow simulation, which will be fed into finite element models such as Abaqus for geomechanics calculations. However, this *one-way coupling* does not update the pressure and displacement back and forth, between the flow and geomechanics calculations at each time step. That is, the dependency between the two equations is not well represented. Thus the result from the coupling computation of STARS is anticipated to be more accurate.

In this study, we will compare the displacement results of STARS with that of the finite element solver Abaqus, which obtains its pressure field input as an output of Schlumberger ECLIPSE. Comparisons will be made to check if the two simulators, when both in their *one-way coupling* mode, have results that agree with one another. We will also be interested to see how much STARS can improve the displacement results with its iterative coupling capacity.

Model Comparison on One-Way Coupling

We first simulate the base case of PUNQ in different simulators. Francesca Bottazzi (personal connection) of ENI, Milan, Italy simulates in ECLIPSE the fluid flow of PUNQ. The pressure result generated by ECLIPSE is then fed into the finite element solver Abaqus for geomechanics calculation. This was done because Abaqus does not have a fluid flow simulation component. As ECLIPSE and Abaqus does not iteratively update the pressure and displacement change at each time step, this is indeed a one-way coupling technique. To reflect this one-way operation in STARS, we use a one-way coupling option in our nominal STARS simulation. The operational conditions and pressure results from the CMG and ECLIPSE will be compared. Because the pressure change through time is indeed critical to the surface displacement result, the corresponding results will also be compared. Then the displacement results will be compared between CMG and Abaqus.

STARS Sensitivity Analysis

To observe how sensitive the ground displacement is, we have made several sensitivity runs by varying the computational methods, subsurface properties and setup of the grid. A nominal case is constructed to carry out sensitivity analysis for STARS around this condition. The setup of this nominal case will be briefly introduced below and further discussed in detail in Chapter 4 – Sample Problem (PUNQ). The result of these sensitivity runs will be shown in Chapter 5 –Result.

Please note that downward displacement in the z-direction is denoted negative, while rightward displacement in the x-direction is denoted positive and upward displacement in the y-direction is denoted negative.

Iterative Coupling vs. One-Way Coupling

We are interested to see if iterative coupling makes a difference in terms of the outcome of the simulation. This computational method is supposed to yield more accurate displacement result of the formation. Given the two coupling methods, we will compare how the surface displacement differs in all directions. Iterative coupling are used throughout the rest of the sensitivity runs.

Sensitivity to Permeability

We run several runs to see how sensitive the ground surface displacement is to the permeability of the reservoir. For simplicity, the permeability field of the nominal case is increased and decreased by 20% as the high permeability and low permeability case respectively. We then compare the results on an earlier date, January 1, 1976, to ensure that the wells have the same production rates among all cases. Please note that the permeability is heterogeneous in all directions in all cases.

To further amplify the effect of high permeability of the formation has on the surface displacement, we also multiply the permeability by 10 times and compare the ground deformation results with those of the nominal case at the end date of the simulation (July 1, 1983).

Sensitivity to Young's Modulus

To test the sensitivity of the ground deformation to rock compressibility, we modify not only the Young's modulus but also the porosity, as the two are related, but we keep the rock matrix compressibility. For the high Young's Modulus case, the porosity of the reservoir is increased by 20%, from 0.15 in the nominal case to 0.18. In the low Young's Modulus case, the porosity is decreased by 20%, from 0.15 in the nominal case to 0.12. The Young's

Modulus from the sensitivity cases are also adjusted accordingly, given that $E = \frac{(1-2\nu)(1+\nu)}{\emptyset\, C_m(1-\nu)} = [kPa]$ where C_m is the rock matrix compressibility $[kPa^{-1}]$, ν is the Poisson's Ratio, and $\emptyset$ is the porosity.

To compare the ground deformation with the same production rates of all wells among all cases (high, nominal and low compressibilities), we choose January 1, 1975 as the date of comparison.

Sensitivity to the Depth of the Reservoir

Lastly, we would like to see how sensitive the ground displacement is to the depth of the reservoir. To amplify the difference, we moved the reservoir up by at least 1350m. Just like other sensitivity runs, the same kind of boundary condition is still imposed.

Chapter 4 – Sample Problem (PUNQ)

General Features

PUNQ is an example problem used in a case study at Imperial College (Imperial College), based on a real field operated by Elf Exploration Production. PUNQ is used because it is a relatively small field to be implemented as a subject of comparison. PUNQ has a dimension of $19 \times 28 \times 5$ blocks, in which 899 blocks are deactivated to capture the irregular shape of the formation.

Setup of the Nominal Case

Modifications Made to the Imperial PUNQ Case

For each layer of PUNQ, the permeabilities along the x- and y- directions are the same while that along the z-direction is different. Also, every layer of PUNQ has a distinct permeability field.

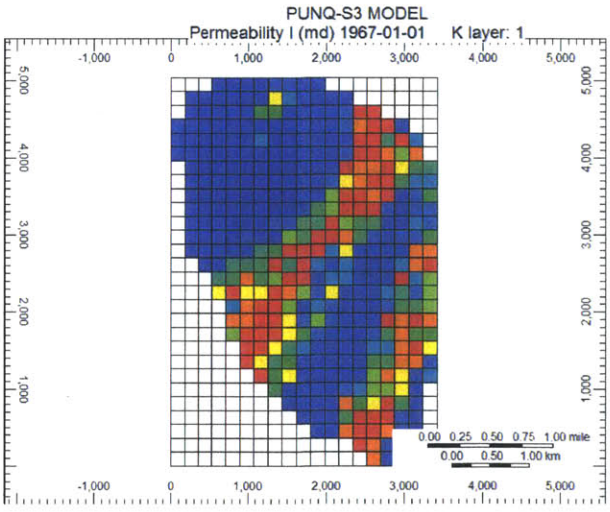

Figure 6 An example of the heterogeneity of PUNQ's permeability (Layer 1, along the x-direction)

In addition, the original porosity field has been replaced by a constant value. In the base case of this study, the porosity is designated as 0.15 throughout the whole field.

The original PUNQ case study by Imperial College has an aquifer which lay beneath the oil reservoir. However, in this study, this aquifer had been removed. Also, the compressibility of rock is modified from $4.5 \times 10^{-6} kPa^{-1}$ to $4.5 \times 10^{-5} kPa^{-1}$. It is increased by an order of

magnitude so as to enhance the observability of the displacement effect during well operation.

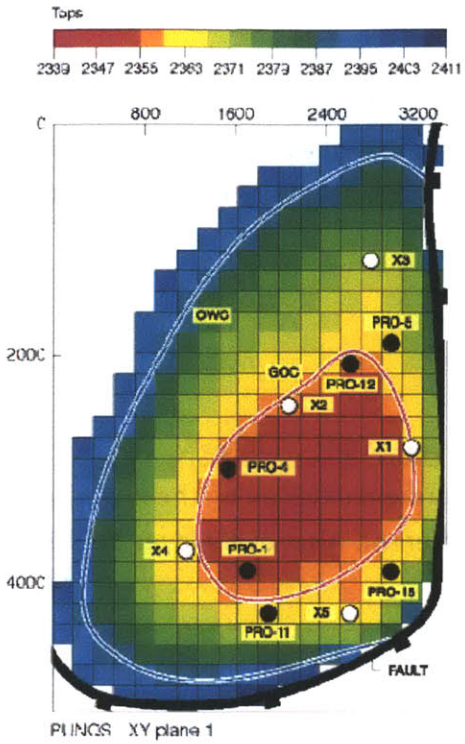

Figure 7 Anaerial view of PUNQ shown with the distribution of wells and its geological structure (please note that the view is flipped in the J-direction (Imperial College)

As seen in Figure 7, the peripheral area of original PUNQ was partly bounded by a fault. Given the fault, a discontinuity along the edge of the formation exists, as shown in Figure 8. Although such a discontinuity would not cause problems during the finite volume computation of fluid flow, issues may arise during the finite element computation of geomechanics. In order to avoid them, the original grid blocks which show discontinuity are smoothed out (Imperial College).

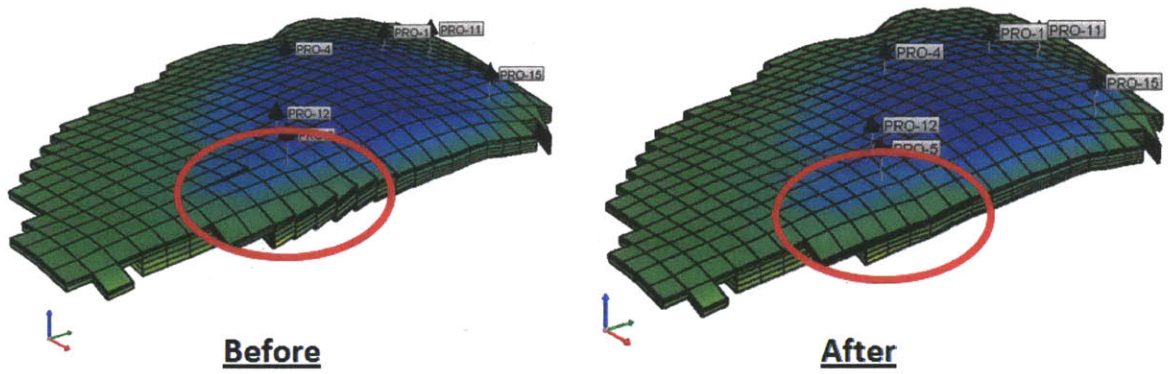

Figure 8 The discontinuity of the original PUNQ structure has been smoothed out to avoid computational issues

Modifications Made to Production Schedule

We modify the original production schedule set up by Imperial College in order to emphasize the displacement result. The original schedule by Imperial College has a periodic change of production rate. Starting from 1972, on January 1 of each calendar year the production rate drops from 150 cubic meters per day to zero cubic meter per day within an one-day time period. Then on January 15 of each year, the production rate would go back to 150 cubic meters per day. Please refer to Figure 9 below for changes made to the schedule by Imperial College. The periodic change of production rate is shown with more detail in the "zoomed-in" box.

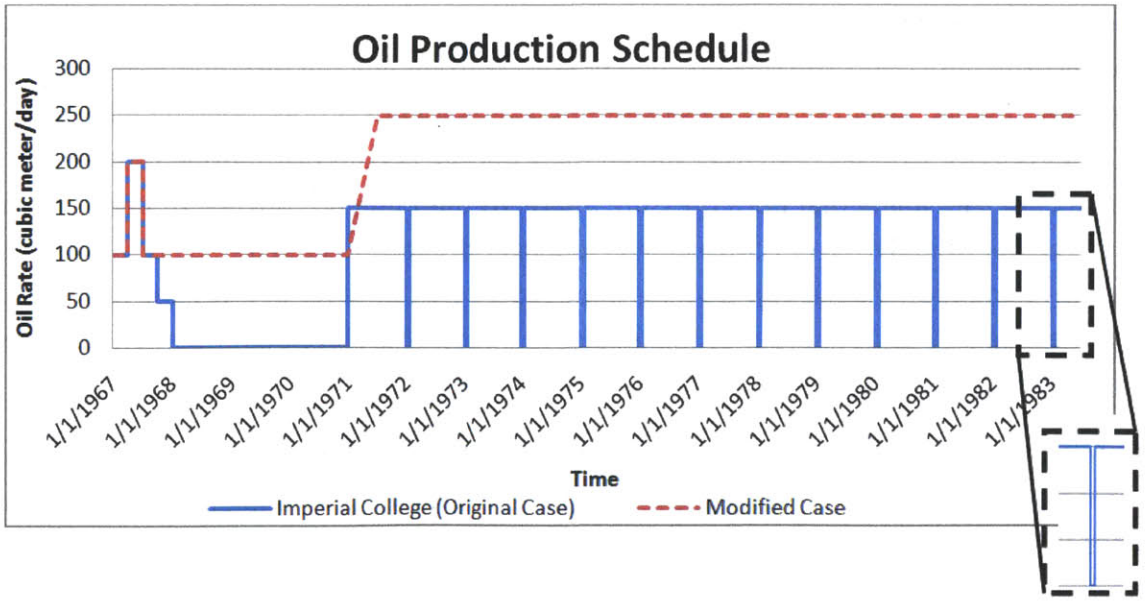

Figure 9 Difference between the schedule of PUNQ in our base case and that originally provided by Imperial College.

Operational Constraints

In the simulators Schlumberger ECLIPSE and CMG STARS, the minimum well bottom-hole pressure (WBHP) of 12000 kPa is set as the operational constraint. In the original case, the oil production rate of a well is to be cut by a percentage of 25% just to ensure that its WBHP is at or above the 12000 kPa minimum. In our modified case, each well will continue to operate. It adjusts its production rate by reducing it as long as the WBHP hits the 12000 kPa minimum, but without an enforced cutback rate.

Geomechanics Grid Setup: Difference between CMG and Abaqus

Due to the different nature of STARS and Abaqus, the geomechanics grids use in the two simulators were different, especially for the thicknesses of the grid layers. This is because in Abaqus users can specify which part of the grid is governed by geomechanics and which part of the grid is the reservoir and governed by not only geomechanics but also by fluid flow. In STARS, such differentiation is automatically detected by the software. Nevertheless, it is hard to ensure that fluid flow equations are properly applied to the corresponding grids.

Theoretically, at the interface between the reservoir grids (porous) and non-reservoir grids (non-porous), pore pressure drops suddenly to zero pore pressure. Given the sudden change of pore pressure, this would affect the total stress and effective stress, which should drop abruptly across the porous and non-porous interface.

In STARS, across the interface the pore pressure drops to zero as it should. However, the total stress and effective stress do not drop in the same manner. Instead of having the porous and non-porous boundary as the interface of sudden drop of stresses, these stresses gradually drop until it hits the second layer of grids surrounding the reservoir grids. This means that the first layer of grids outside of the reservoir grids is prescribed with higher total and effective stresses than they should theoretically. So this distribution of stress is "smeared out", meaning that pore pressure indirectly has influence outside of the reservoir. Because higher effective stress corresponds to bigger displacement in any grids (as in the constitutive Equation 8 page 10), we have imposed a very thin layer of grids above and below the reservoir grids in order to minimize this effect. Therefore our grid in STARS is set up differently (Figure 11).

In Abaqus, users can specify whether the grids belong to the reservoir. Pore pressure has no influence outside of the reservoir grids at all. Therefore we impose simpler grid layering in Abaqus (Figure 10).

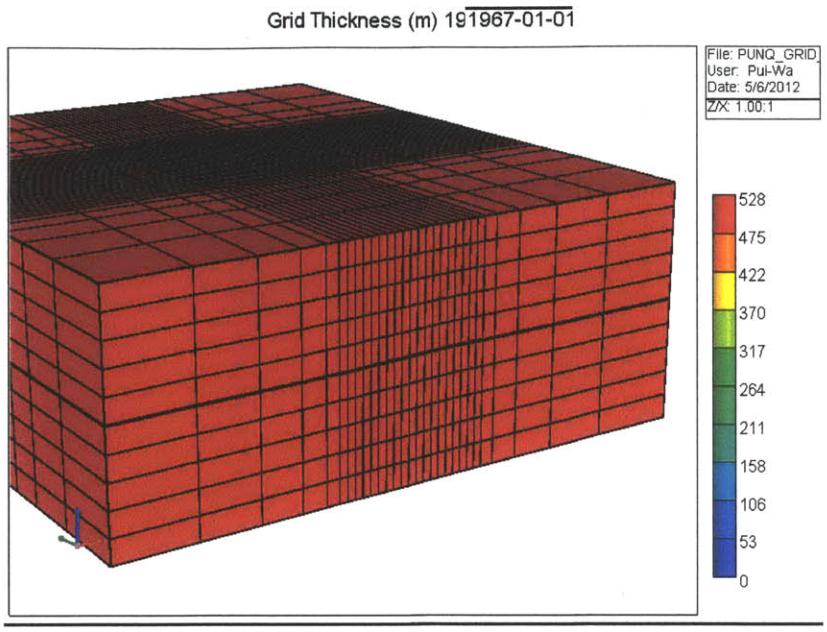

Figure 10 Layering of Abaqus grid: 5 layers of constant thicknesses each for the overburden, reservoir, and underburden

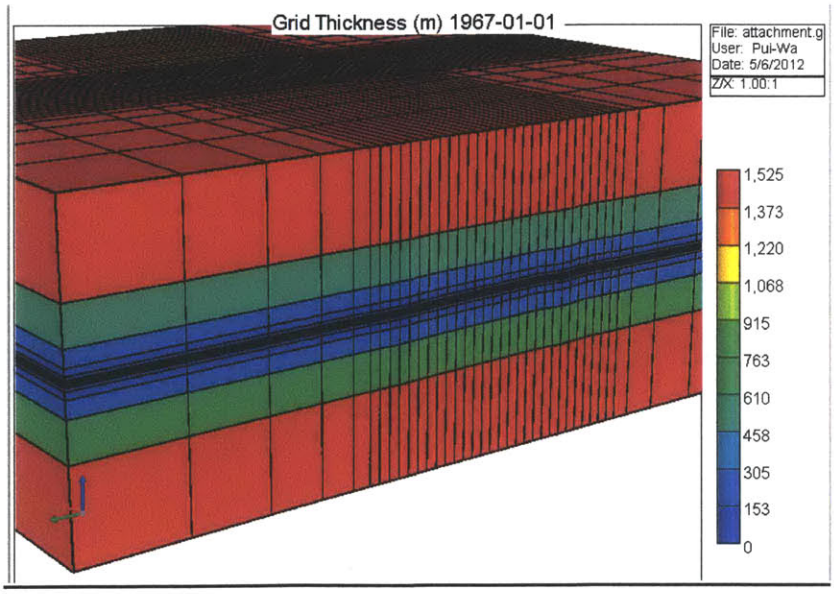

Figure 11 Layering of CMG STARS geomechanics grid: Layers above (overburden) and below (underburden) the 5 reservoir layers (in the middle of the geomechanics grid) have their thicknesses logarithmically scaled.

Dates of Comparison

Here we have chosen seven particular dates to show the pressure field results. These dates correspond to different operational conditions during the simulation or WBHP. They are

January 1, 1967, January 1, 1970, January 15, 1972, January 1, 1974, January 1, 1977, January 1, 1981, and July 1, 1983.

For the displacement result of the sensitivity analysis, only the end date of the simulation is shown (i.e., July 1, 1983). This is the same for the displacement field comparison between CMG and Abaqus.

Chapter 5 – Model Comparison Results

Well Operating Conditions in STARS and ECLIPSE

Here the operational conditions simulated at each well are compared (Figures 12 to 17). For most wells, the results on the oil production rates and WBHP between CMG and ECLIPSE are similar. However, well Pro-12 shows a more noticeable difference between the two simulators. This could be due to different well models in CMG and ECLIPSE.

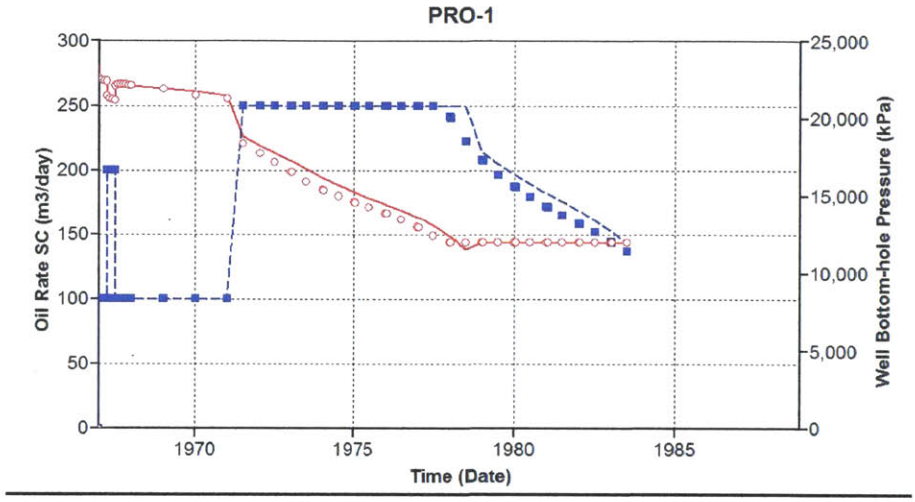

Figure 12 Well Pro-1: Oil production rates (in blue) and WBHP (in red) results of the CMG (connectedpoints) and ECLIPSE (unconnected points)

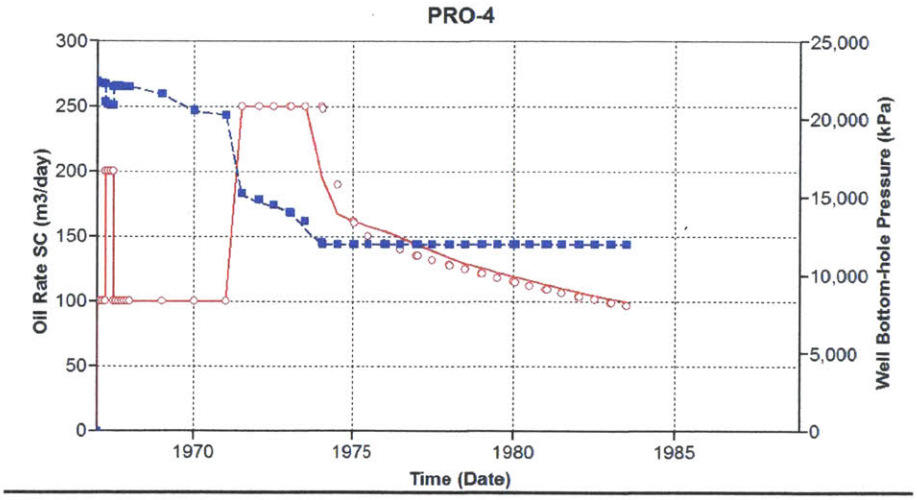

Figure 13 Well Pro-4: Oil production rates (in blue) and WBHP (in red) results of the CMG (connected points) and ECLIPSE (unconnected points)

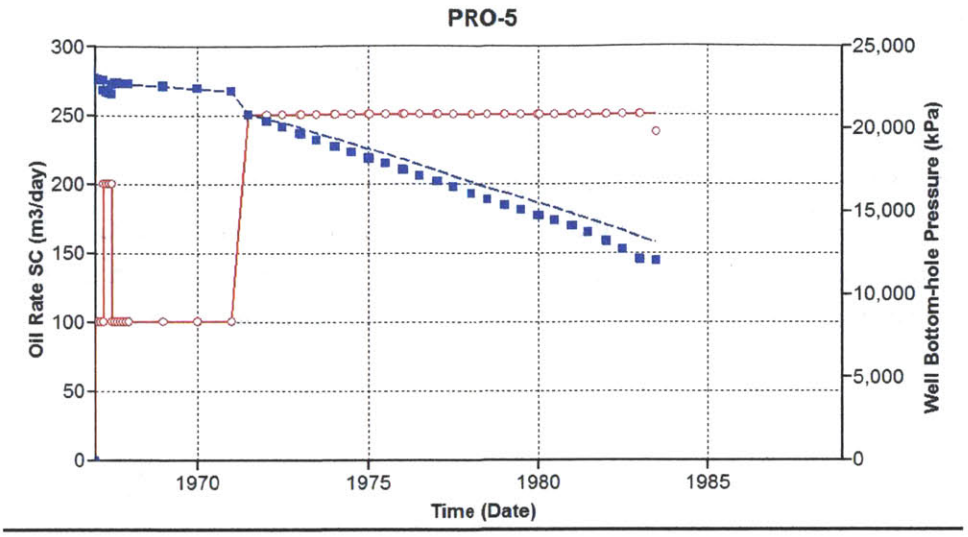

Figure 14 Well Pro-5: Oil production rates (in blue) and WBHP (in red) results of the CMG (connected points) and ECLIPSE (unconnected points)

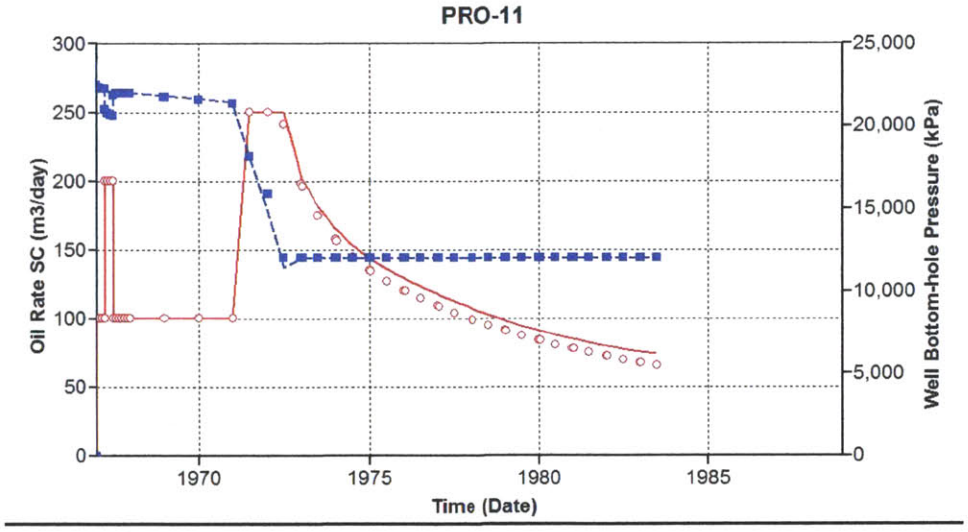

Figure 15 Well Pro-11: Oil production rates (in blue) and WBHP (in red) results of the CMG (connected points) and ECLIPSE (unconnected points)

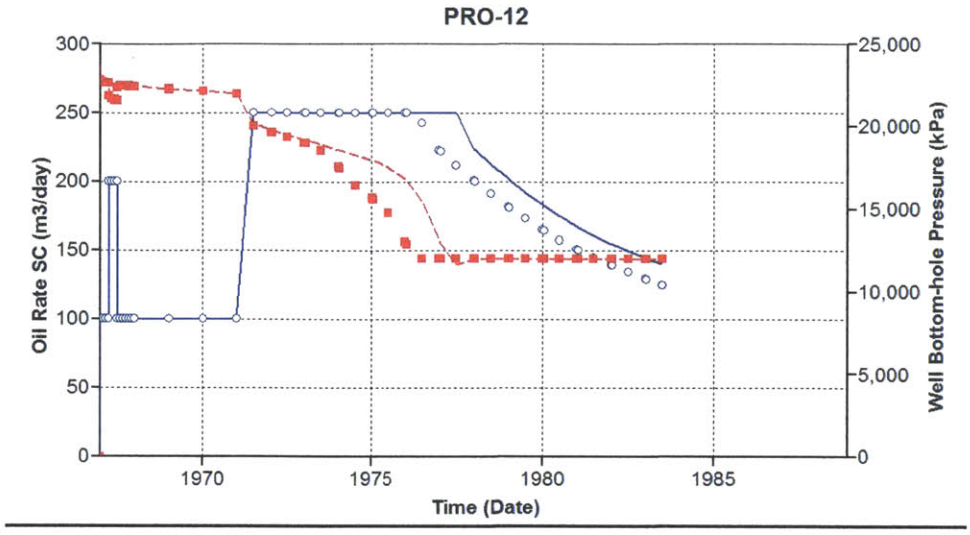

Figure 16 Well Pro-12: Oil production rates (in blue) and WBHP (in red) results of the CMG (connected points) and ECLIPSE (unconnected points)

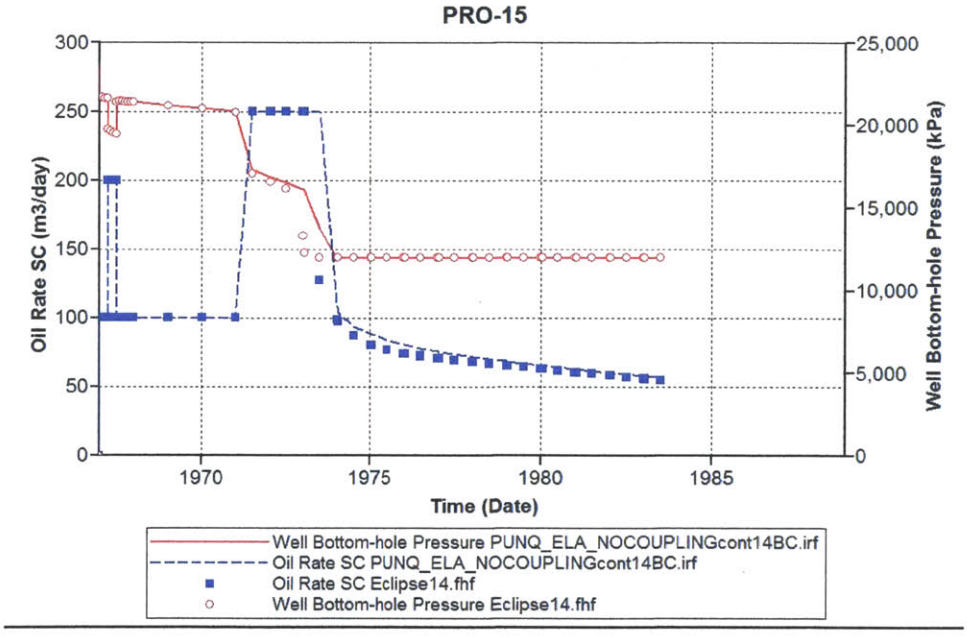

Figure 17 Well Pro-15: Oil production rates (in blue) and WBHP (in red) results of the CMG (connected points) and ECLIPSE (unconnected points)

Pressure Field Results from STARS and ECLIPSE

In this section, we will discuss the pressure field and displacement field results from the simulation we run on STARS.

Figure 18 to Figure 24 plot the pressure field on those seven dates, so as to compare how the pressure differs between the two simulators. The first row of each figure represents the results from Eclipse, the second row represents those from STARS, and the last row the difference between the pressure fields of the 2 simulators on the same reservoir grid layer (where $P_{difference} = P_{CMG} - P_{Eclipse}$).

The pressure fields between Eclipse and STARS are close, with the pressure of Eclipse lower than that of CMG by 1%. The two simulators seem to agree rather well with each other in the flow simulation; but we are yet to see how this pressure difference from one simulator to another will lead to differences in the displacement field.

Because of that, it is more important to compare the pressure change of the reservoir through time. Referring back to the constitutive equation (Equation 8 on Page 8), pressure changes through time have a substantial implication for the deformation of the geomechanics grid. Therefore, from Figure 25 to Figure 30, the pressure change of the reservoir layers with respect to time 0 were shown.

The pressure change with time result shows that, by the end of the simulation, the difference between the results of the two simulators has increased up to 10% of the total pressure change in Eclipse. This difference in pressure could be due to many factors, including different well models used in the simulators.

Nevertheless, we should look into the displacement comparison between CMG and Abaqus. As bigger pressure change through time theoretically corresponds to bigger displacements, it would be interesting to see if Abaqus yields more displacements.

The displacement field simulated by CMG is different from that by Abaqus. This could be due to several factors. First, the geomechanics grid adopts in CMG is different from that in Abaqus. This would change the mesh used in the finite element computation, thus affecting the displacement in the end. Second, if pressure field used at time t was frozen to calculate the displacement from time t to time t+1, this can have an effect on the displacement too. Please refer to Figure 31 to Figure 33 in the next section for the displacement field comparison in x-, y-, and z- directions.

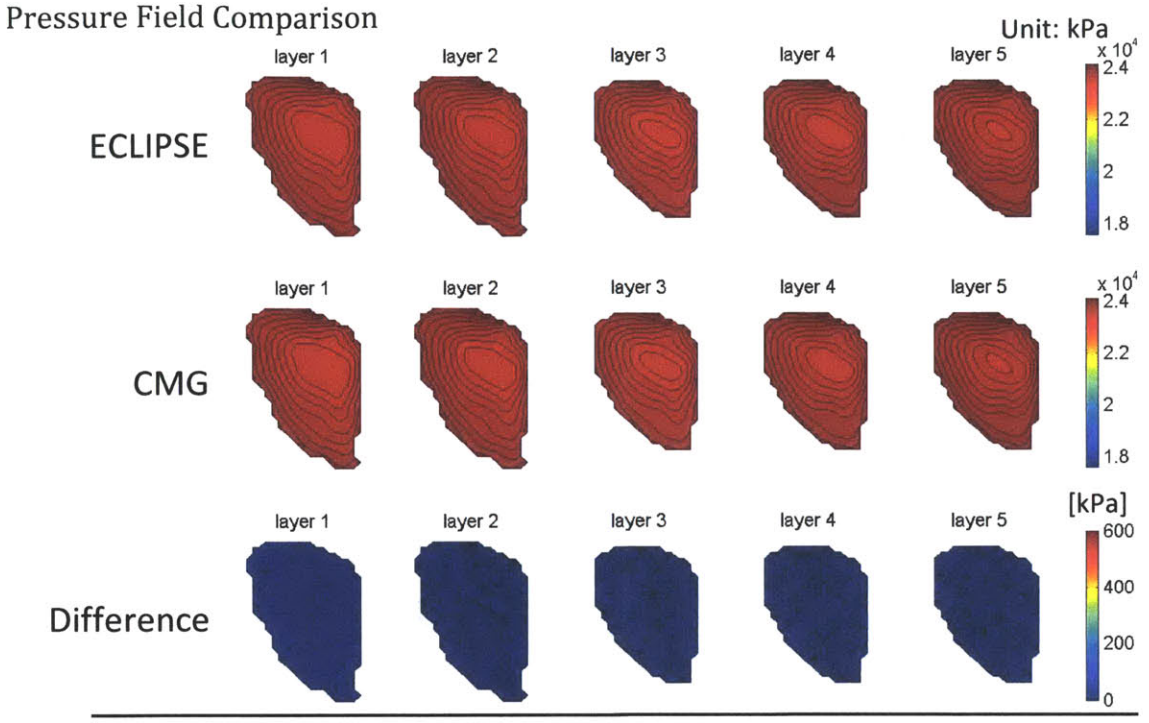

Figure 18 Pressure fields of PUNQ on January 1, 1967 generated by Eclipse, CMG, and the difference of the two (P_difference = P_cmg – P_eclipse) in kPa

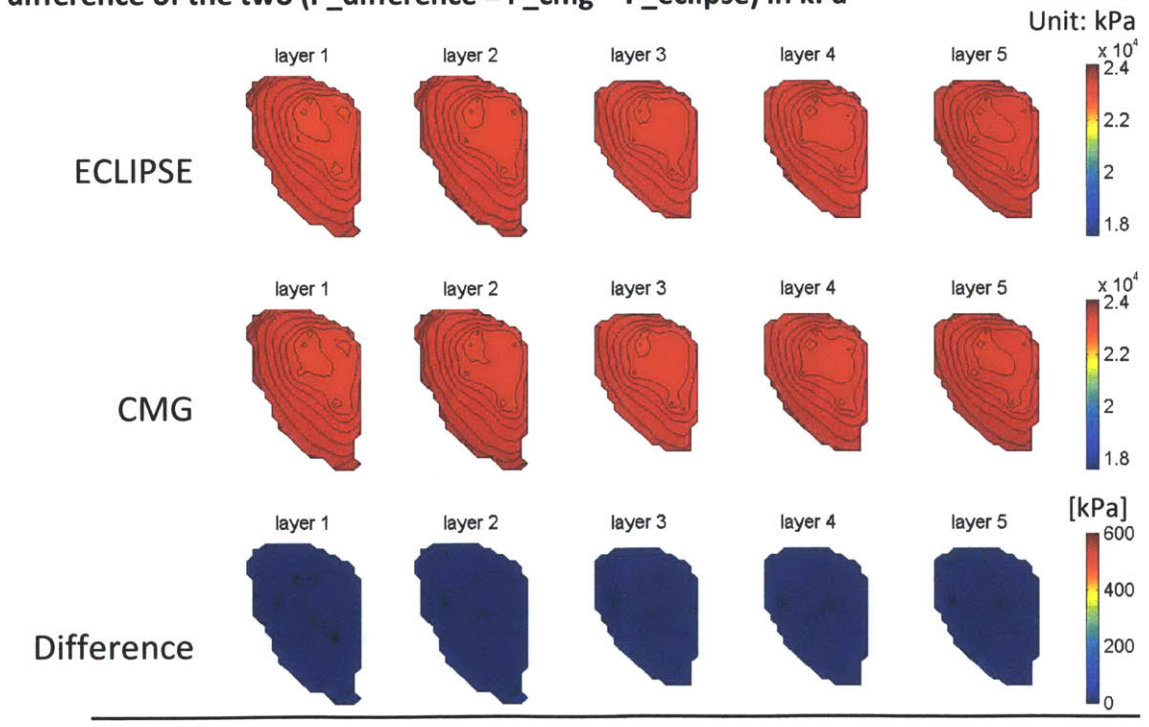

Figure 19 Pressure fields of PUNQ on January 1, 1970 generated by Eclipse, CMG, and the difference of the two (P_difference = P_cmg – P_eclipse) in kPa

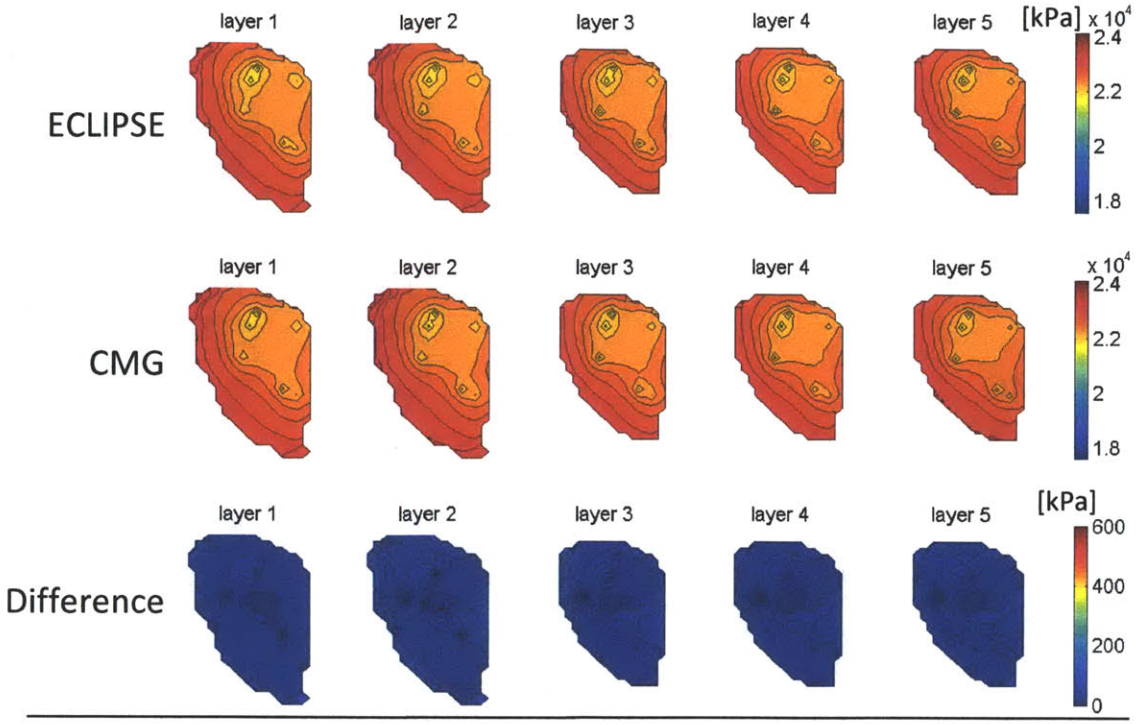

Figure 20 Pressure fields of PUNQ on January 15, 1972 generated by Eclipse, CMG, and the difference of the two (P_difference = P_cmg – P_eclipse) in kPa

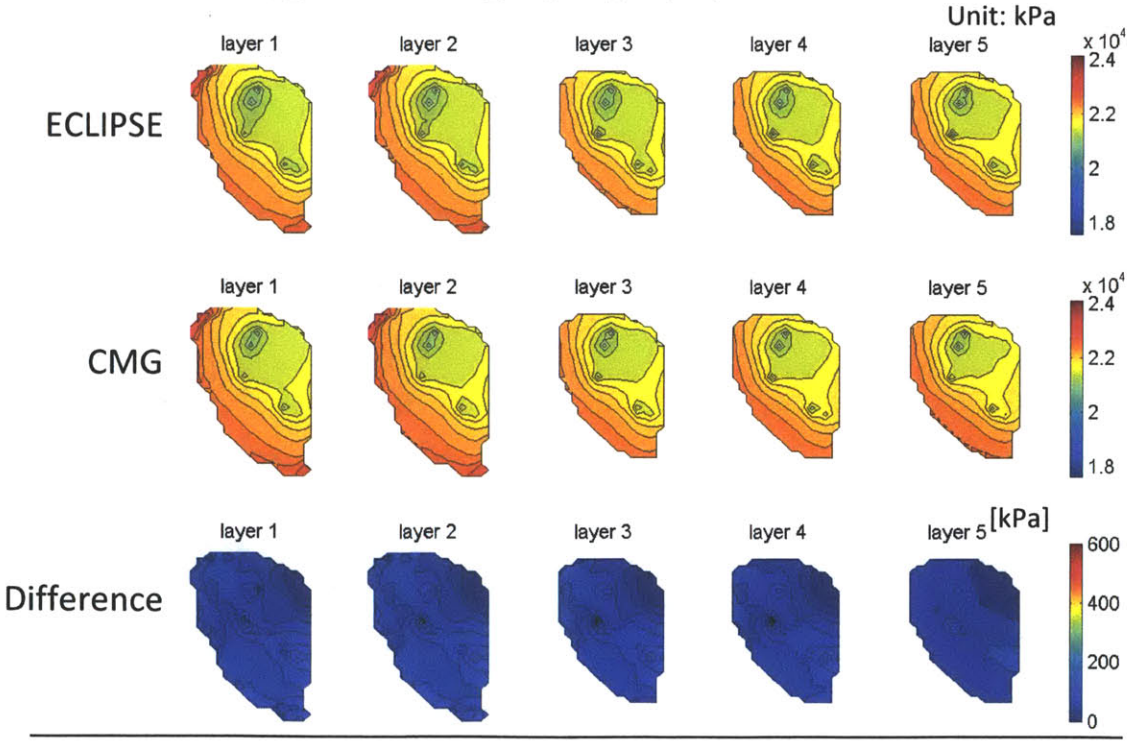

Figure 21 Pressure fields of PUNQ on January 1, 1974 generated by Eclipse, CMG, and the difference of the two (P_difference = P_cmg – P_eclipse) in kPa

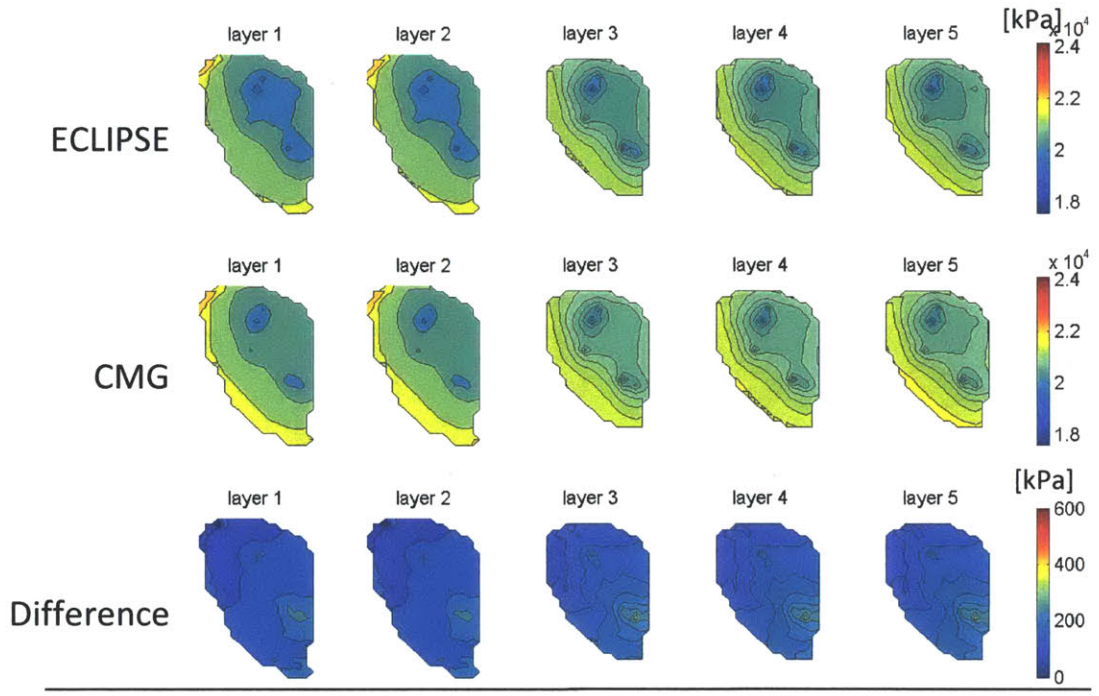

Figure 22 Pressure fields of PUNQ on January 1, 1977 generated by Eclipse, CMG, and the difference of the two (P_difference = P_cmg – P_eclipse) in kPa

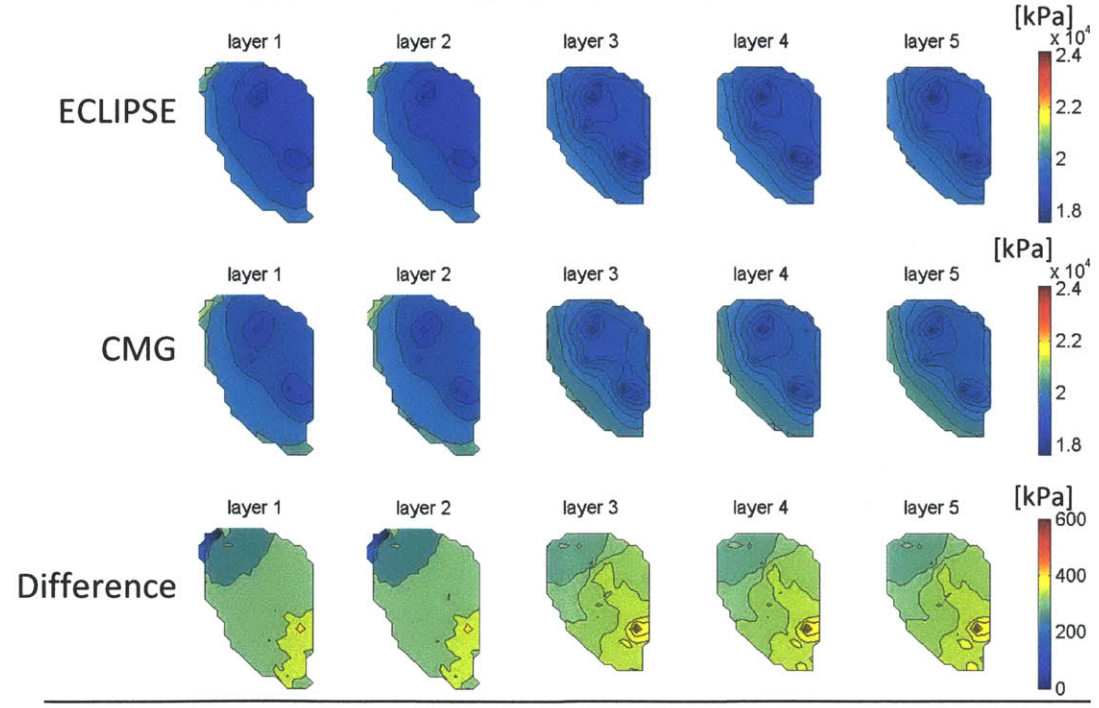

Figure 23 Pressure fields of PUNQ on January 1, 1981 generated by Eclipse, CMG, and the difference of the two (P_difference = P_cmg – P_eclipse) in kPa

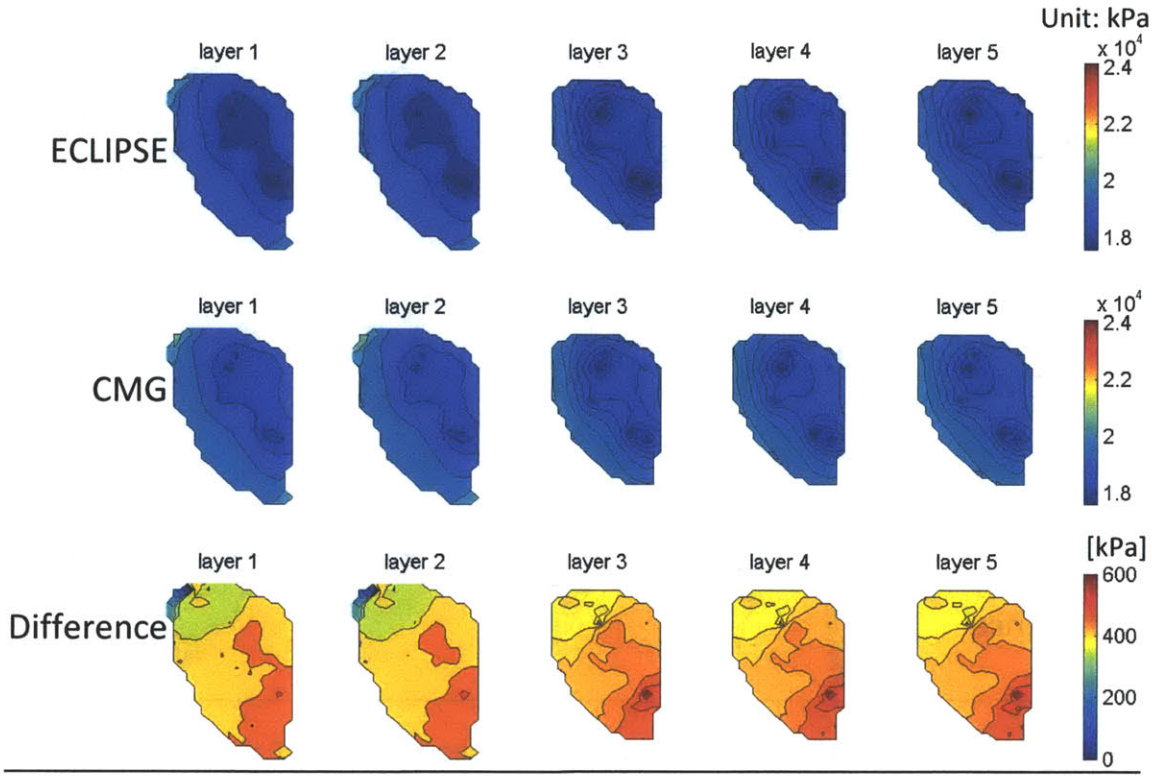

Figure 24 Pressure fields of PUNQ on July 1, 1983 generated by Eclipse, CMG, and the difference of the two (P_difference = P_cmg – P_eclipse) in kPa

Pressure Drop Comparison

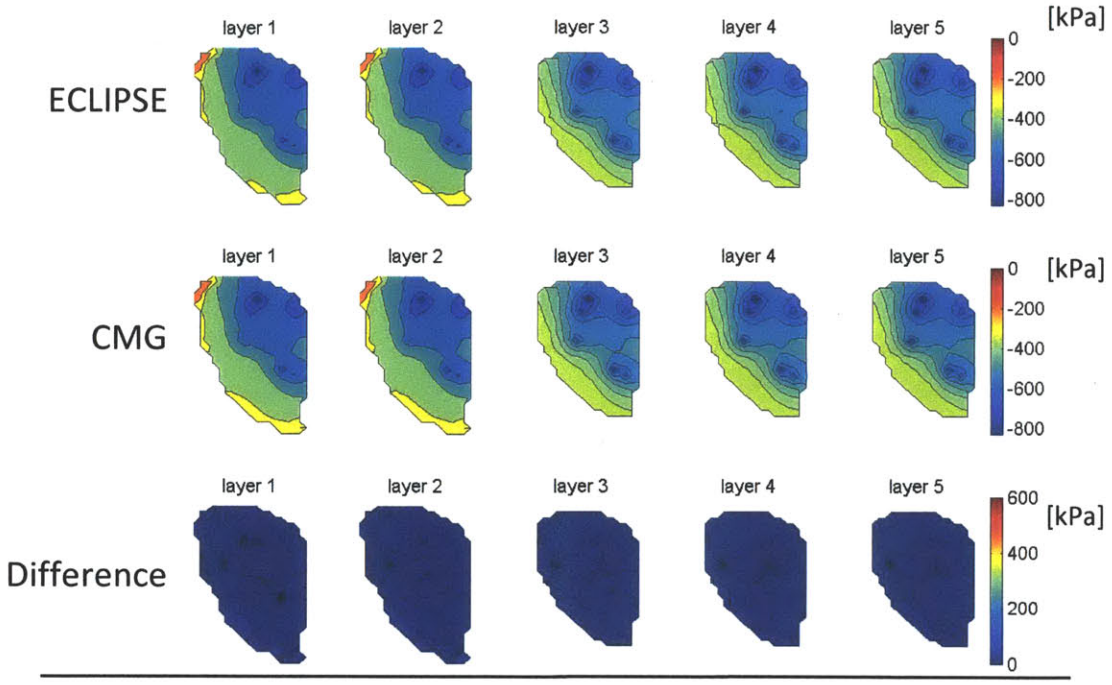

Figure 25 Pressure drop of PUNQ from January 1, 1967 (t = 0) to January 1, 1970 generated by Eclipse, CMG, and the difference of the two (ΔP_difference = ΔP_cmg – ΔP_eclipse) in kPa

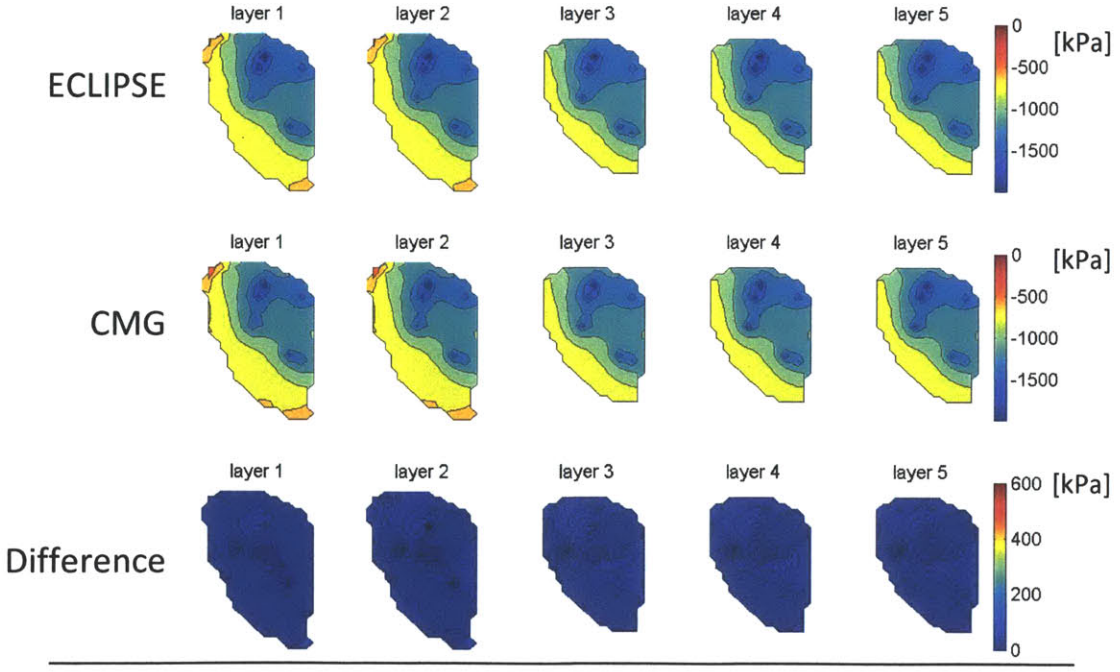

Figure 26 Pressure drop of PUNQ from January 1, 1967 (t = 0) to January 15, 1972 generated by Eclipse, CMG, and the difference of the two (ΔP_difference = ΔP_cmg – ΔP_eclipse) in kPa

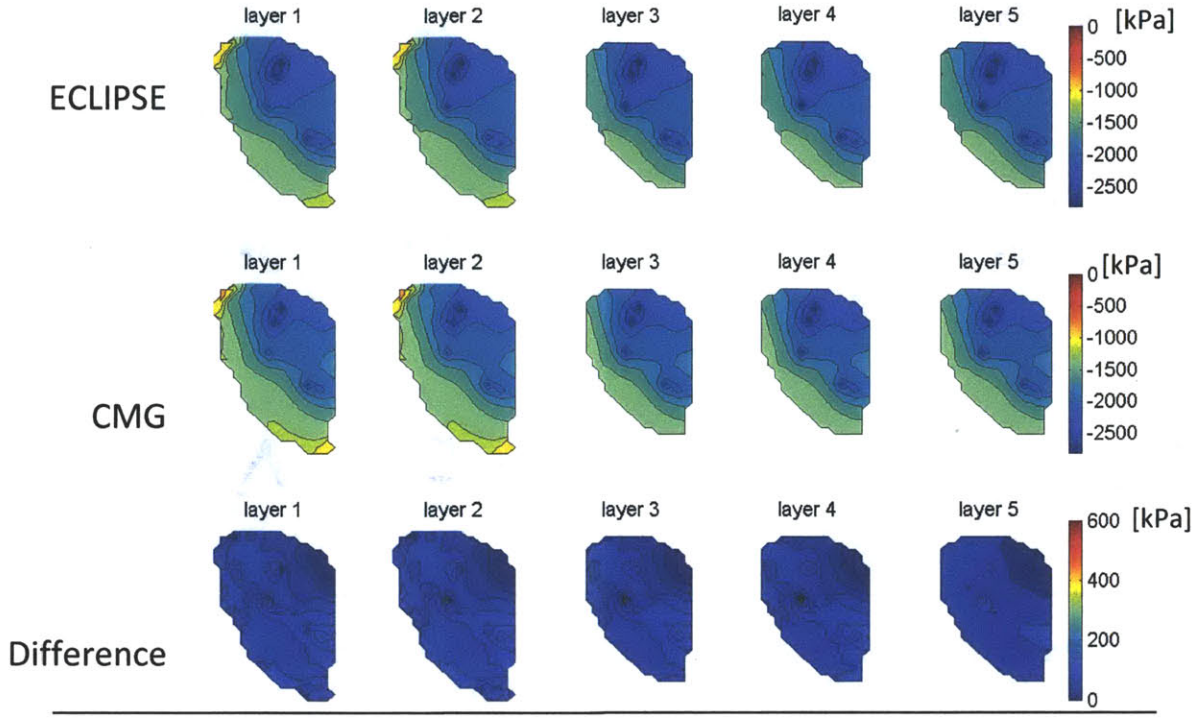

Figure 27 Pressure drop of PUNQ from January 1, 1967 (t = 0) to January 1, 1974 generated by Eclipse, CMG, and the difference of the two (ΔP_difference = ΔP_cmg – ΔP_eclipse) in kPa

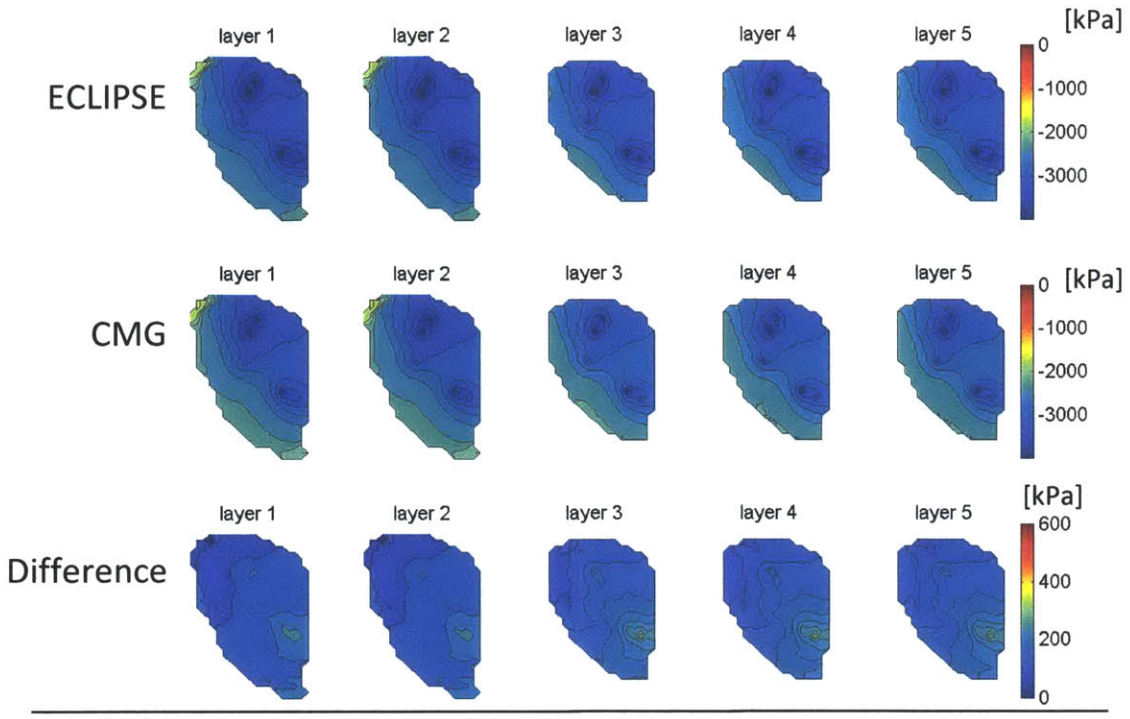

Figure 28 Pressure drop of PUNQ from January 1, 1967 (t = 0) to January 1, 1977 generated by Eclipse, CMG, and the difference of the two (ΔP_difference = ΔP_cmg – ΔP_eclipse) in kPa

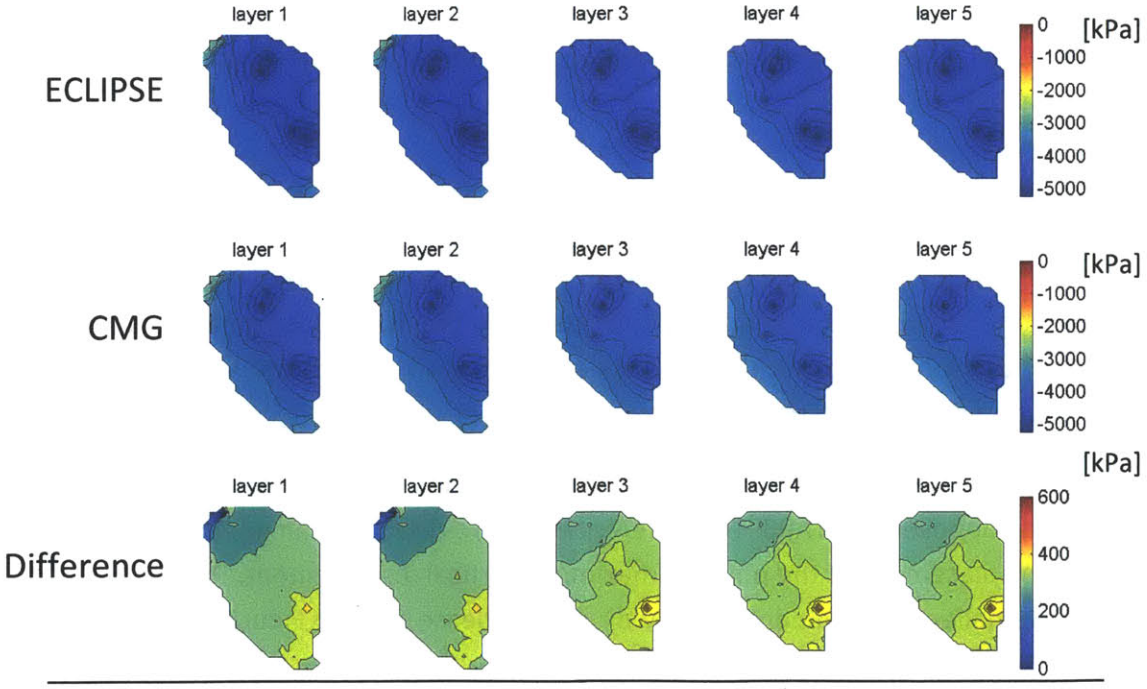

Figure 29 Pressure drop of PUNQ from January 1, 1967 (t = 0) to January 1, 1981 generated by Eclipse, CMG, and the difference of the two (ΔP_difference = ΔP_cmg – ΔP_eclipse) in kPa

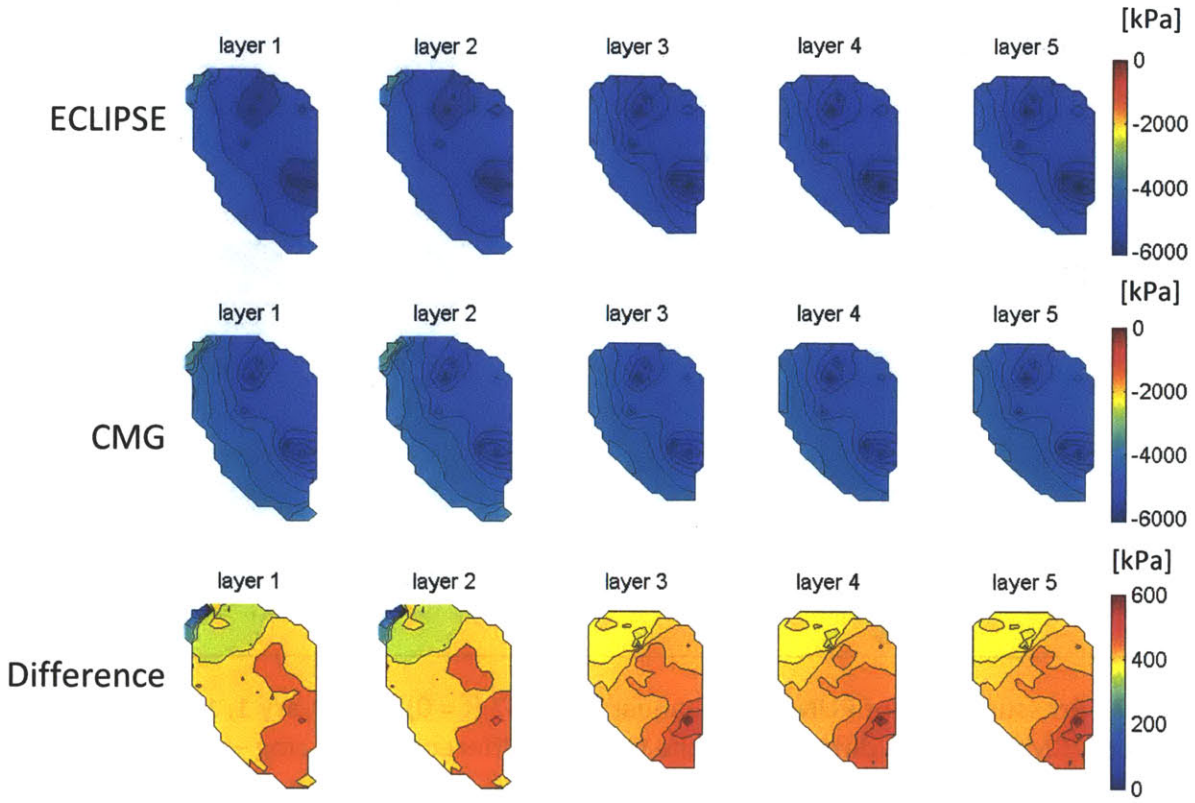

Figure 30 Pressure drop of PUNQ from January 1, 1967 (t = 0) to January 1, 1983 generated by Eclipse, CMG, and the difference of the two (ΔP_difference = ΔP_cmg – ΔP_eclipse) in kPa

Displacement Field Results from STARS and Abaqus

Below are the results comparing the displacement fields generated by STARS and Abaqus. Please note that downward displacement in the z-direction is denoted negative, while rightward displacement in the x-direction is denoted positive, and northward displacement in the y-direction is denoted negative.

The displacement field comparison shows that Abaqus yields small displacements in x- and z-directions as supposed to STARS. The difference in the z-direction can go up to almost 6 to 10% of the displacement at the point of maximum vertical displacement. However, STARS calculates a smaller displacement in the y-direction. Please refer to Figure 31 to Figure 33.

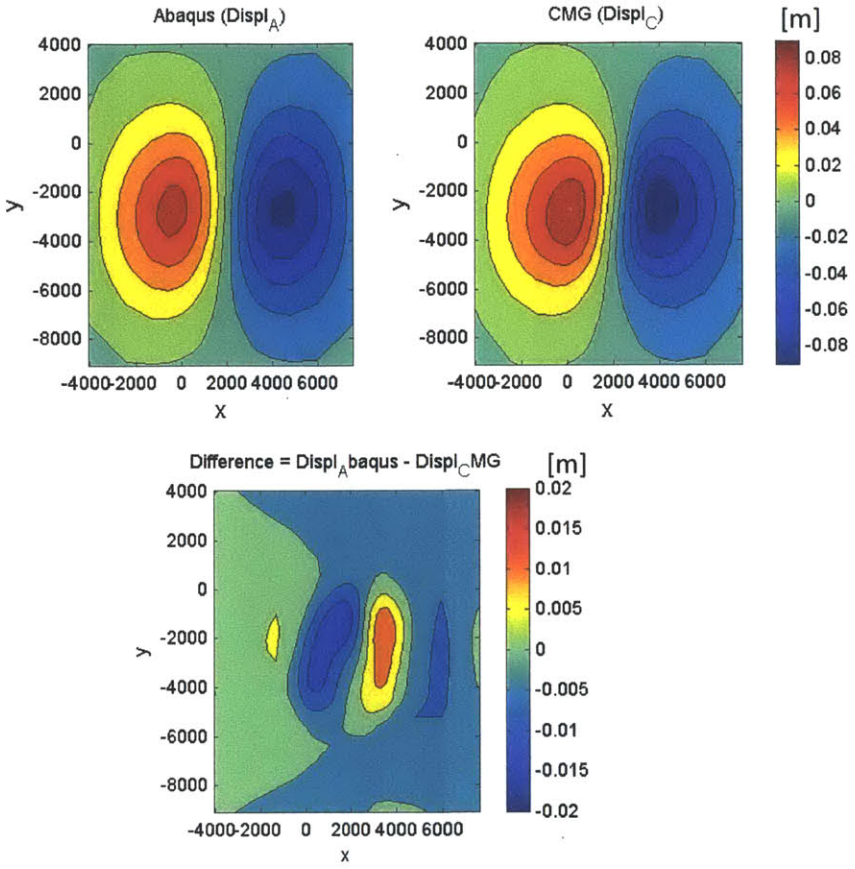

Figure 31 Displacement fields [m] in the x-direction as the output of Abaqus, CMG and the difference (Difference = Ux_CMG – Ux_Abaqus) on the simulation date July 1, 1983

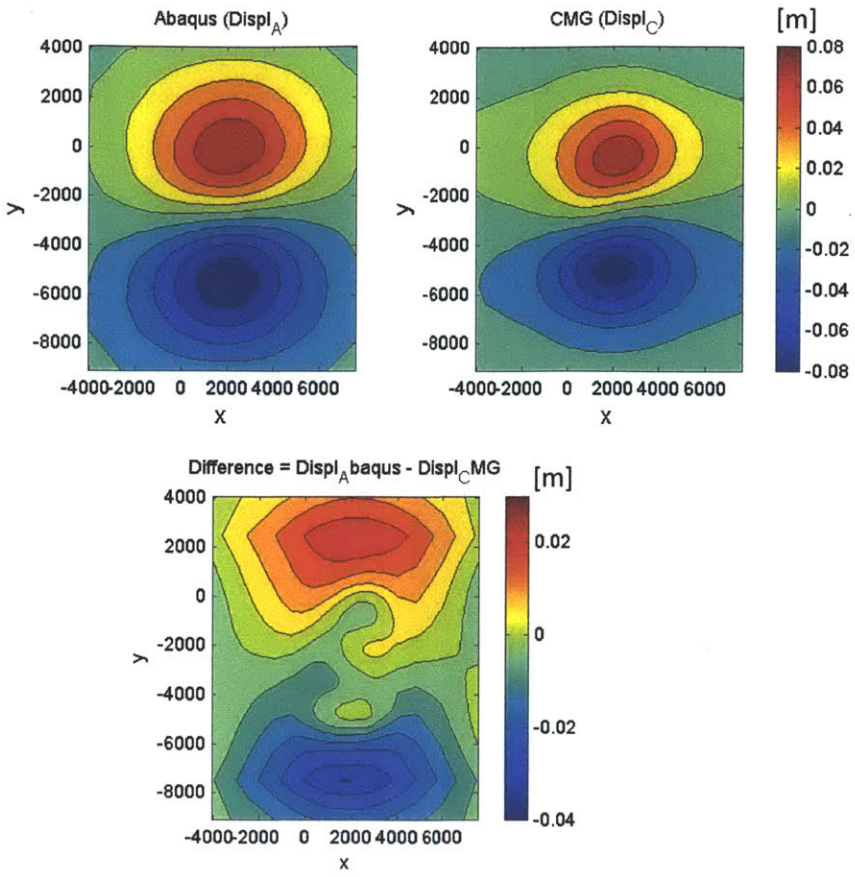

Figure 32 Displacement fields [m] in the y-direction as the output of Abaqus, CMG and the difference (Difference = Ux_CMG – Ux_Abaqus) on the simulation date July 1, 1983

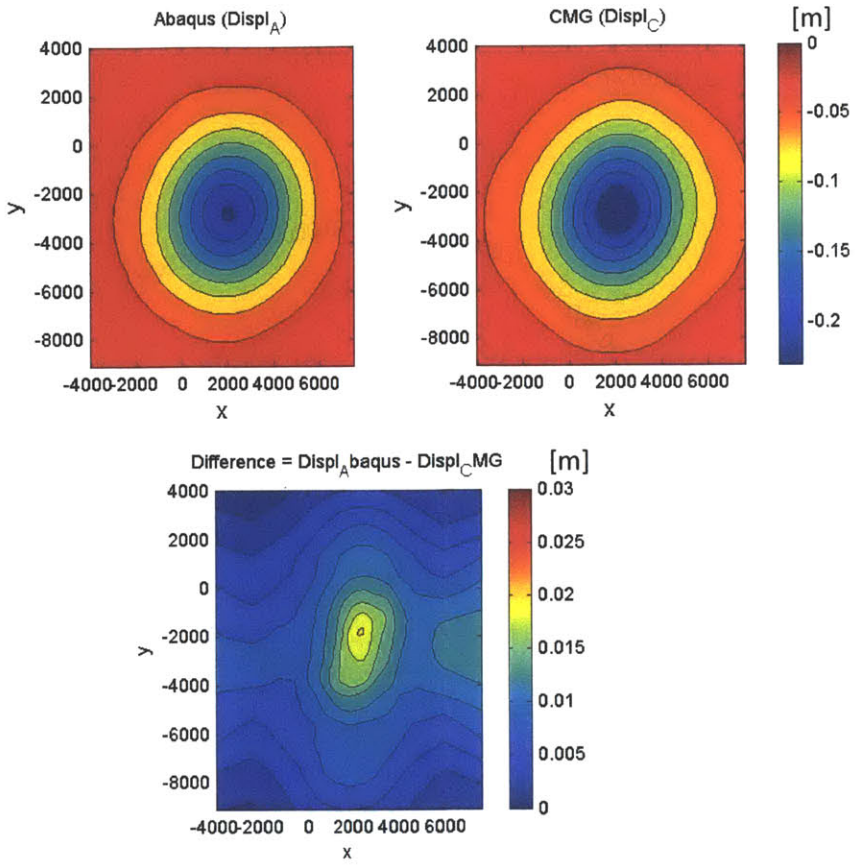

Figure 33 Displacement fields [m] in the z-direction as the output of Abaqus, CMG and the difference (Difference = Ux_CMG – Ux_Abaqus) on the simulation date July 1, 1983

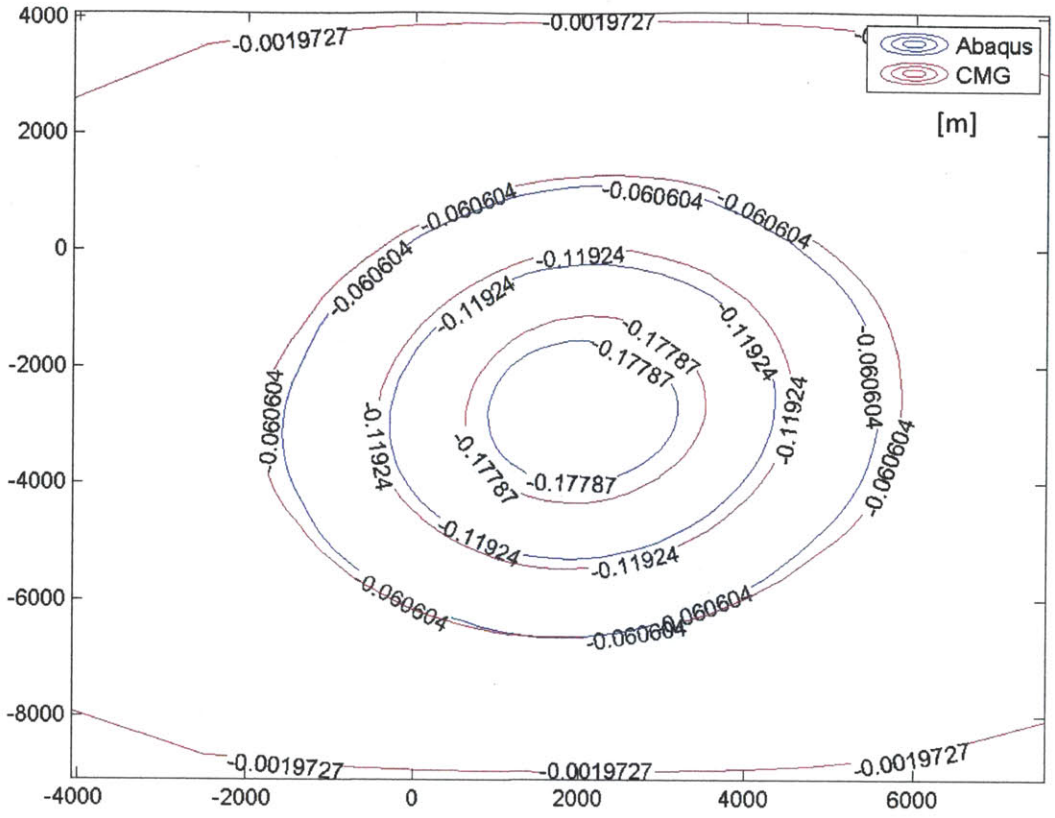

Figure 34 Contours of the displacement fields [m] in the z-direction as the output of Abaqus (blue lines) and CMG (red lines) overlapping each other

Chapter 6 – STARS Sensitivity Result

Iterative Coupling and One-Way Coupling: Displacement Comparison

Figure 35 to Figure 37 show the difference in terms of the displacement results when iterative coupling rather than one-way coupling is used as the computational method in STARS. Iterative coupling is supposed to be more accurate as it updates the pressure and displacement information between the fluid flow and geomechanics equations. Whether it is in the x-, y- and z-directions, the displacement stays the same qualitatively results as in those of one-way coupling but it became qualitatively bigger. That is, the compressive strains in x- and y-directions and the subsidence in the z-direction are calculated as being bigger than before.

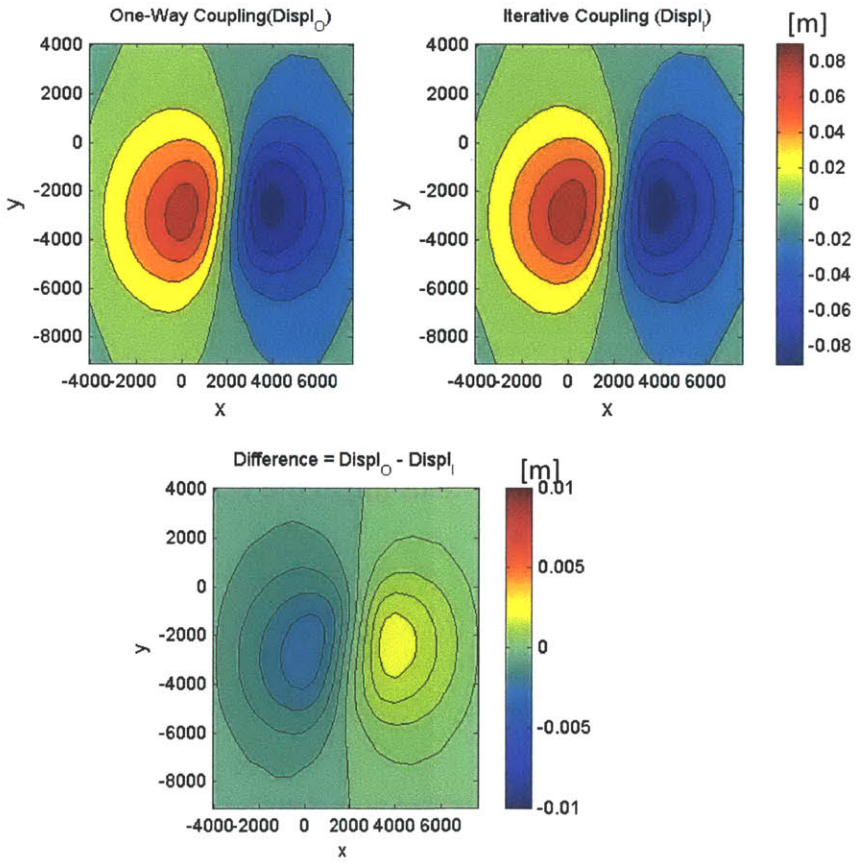

Figure 35 Comparison of the displacement fields [m] in the x-direction as the result of iterative coupling and one-way coupling

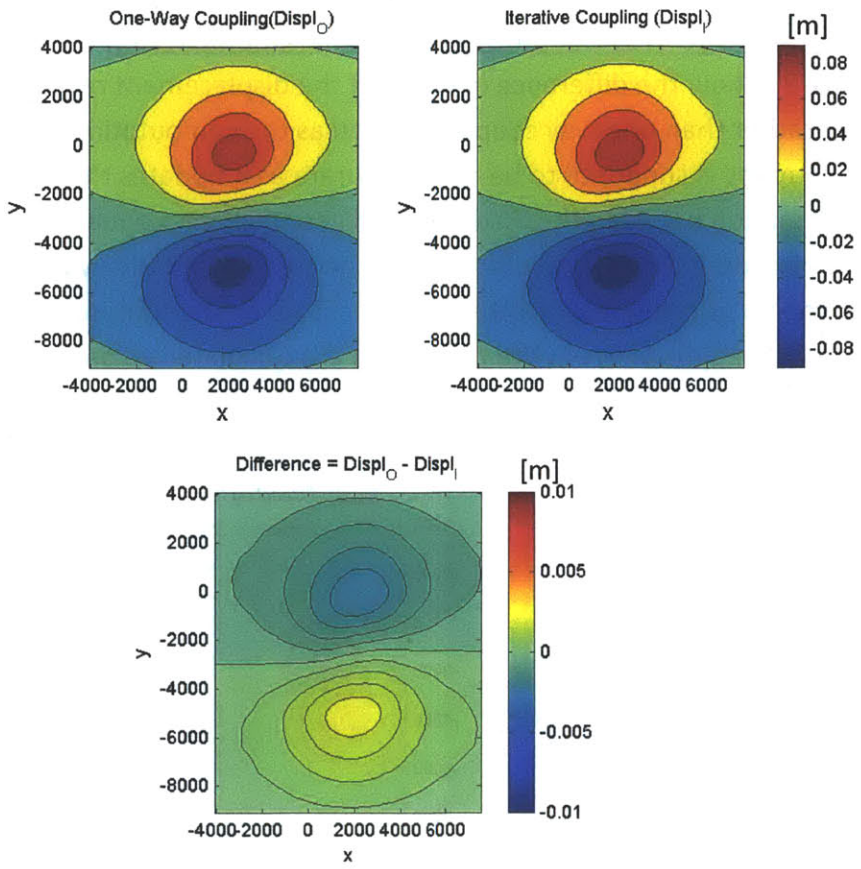

Figure 36 Comparison of the displacement fields [m] in the y-direction as the result of iterative coupling and one-way coupling

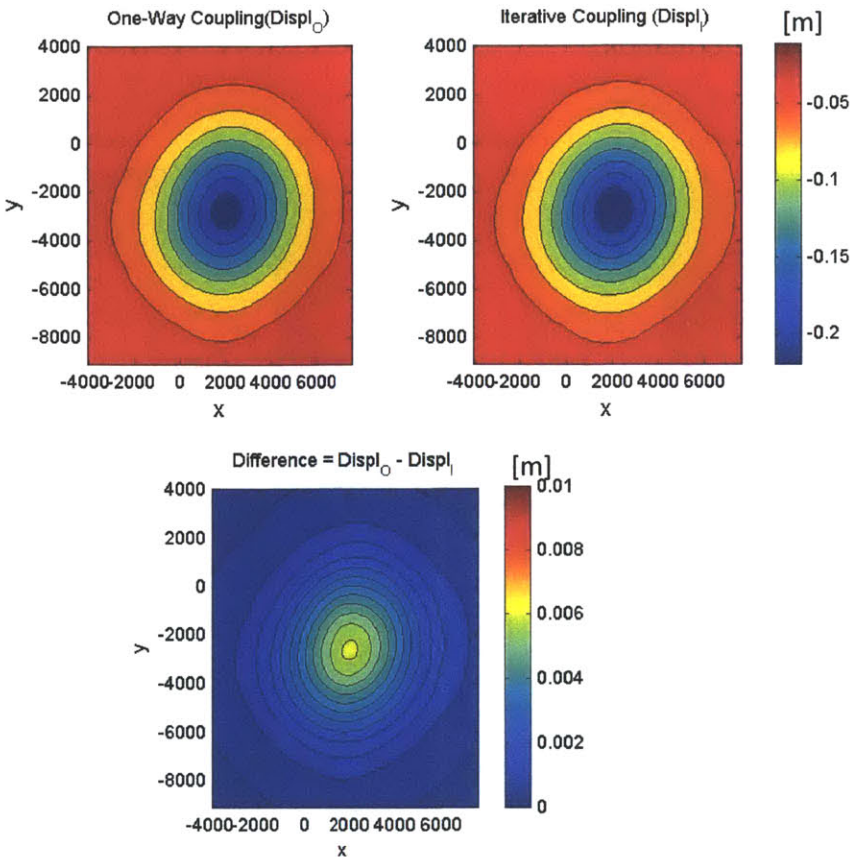

Figure 37 Comparison of the displacement fields [m] in the z-direction as the result of iterative coupling and one-way coupling, in unit of meter

Sensitivity to Permeability

The results of displacement are plotted in Figure 38 to Figure 43. For convenience, the displacement difference between the high permeability case and the nominal and also the displacement difference between the nominal and the low permeability case are plotted on the same figures. So as to compare the three cases with the same production rates in all wells, we compare the ground deformation earlier, on January 1, 1976 (Figure 38 to Figure 40). A more impermeable reservoir does make the ground deformation much less apparent. However on January 1, 1976, the simulation has not taken place long enough to show the difference between the ground deformation in the high permeability and the base permeability case. Therefore a comparison between the two cases is taken for a later date, at the end of the simulation on July 1, 1983 also (Figure 41 to Figure 43). Given a longer

simulation time with a higher overall production level, a highly permeable reservoir does increase the ground deformation.

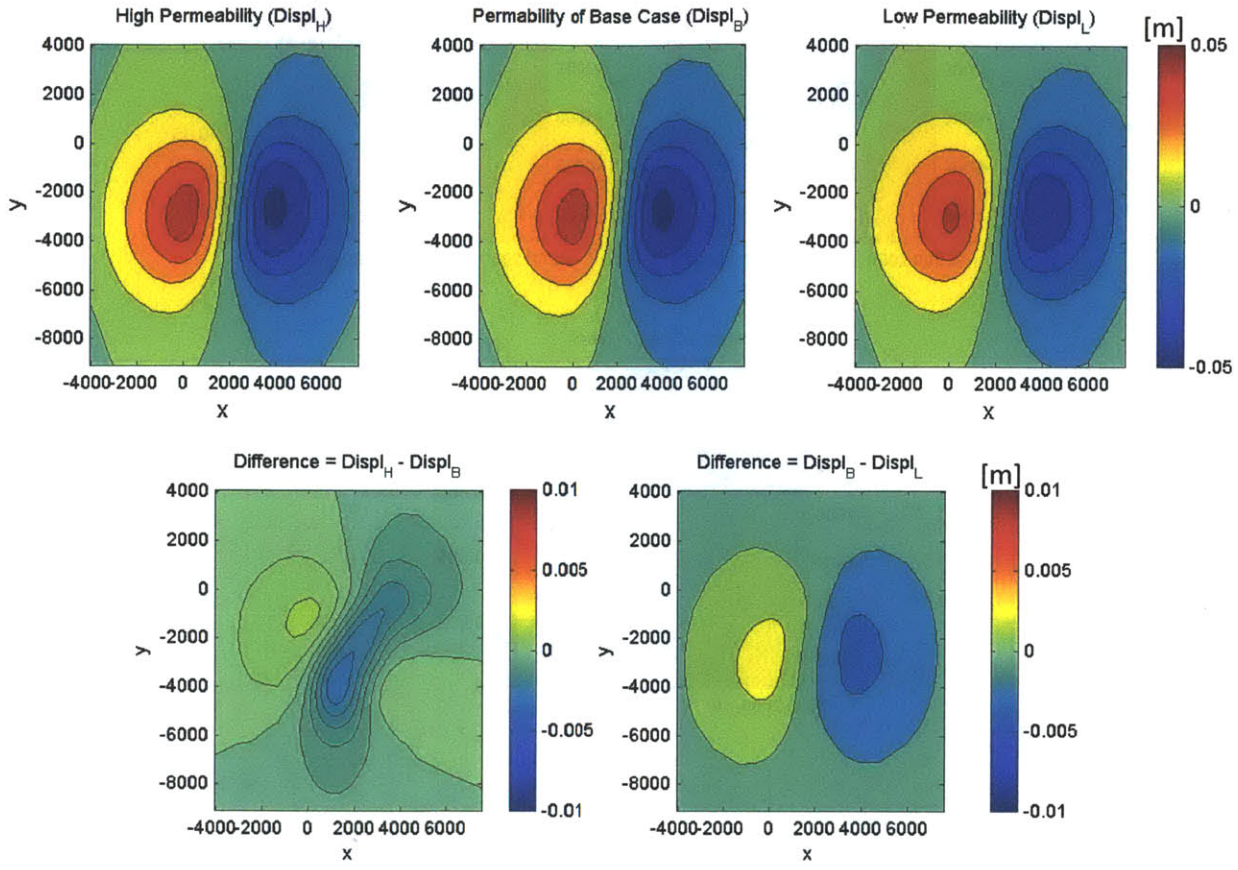

Figure 38 Comparison of the displacement fields [m] in the x-direction on January 1, 1976 when the permeability in all directions is multiplied by 1.2 times (i.e., high permeability) and is 80% of that of the base case (i.e., low permeability)

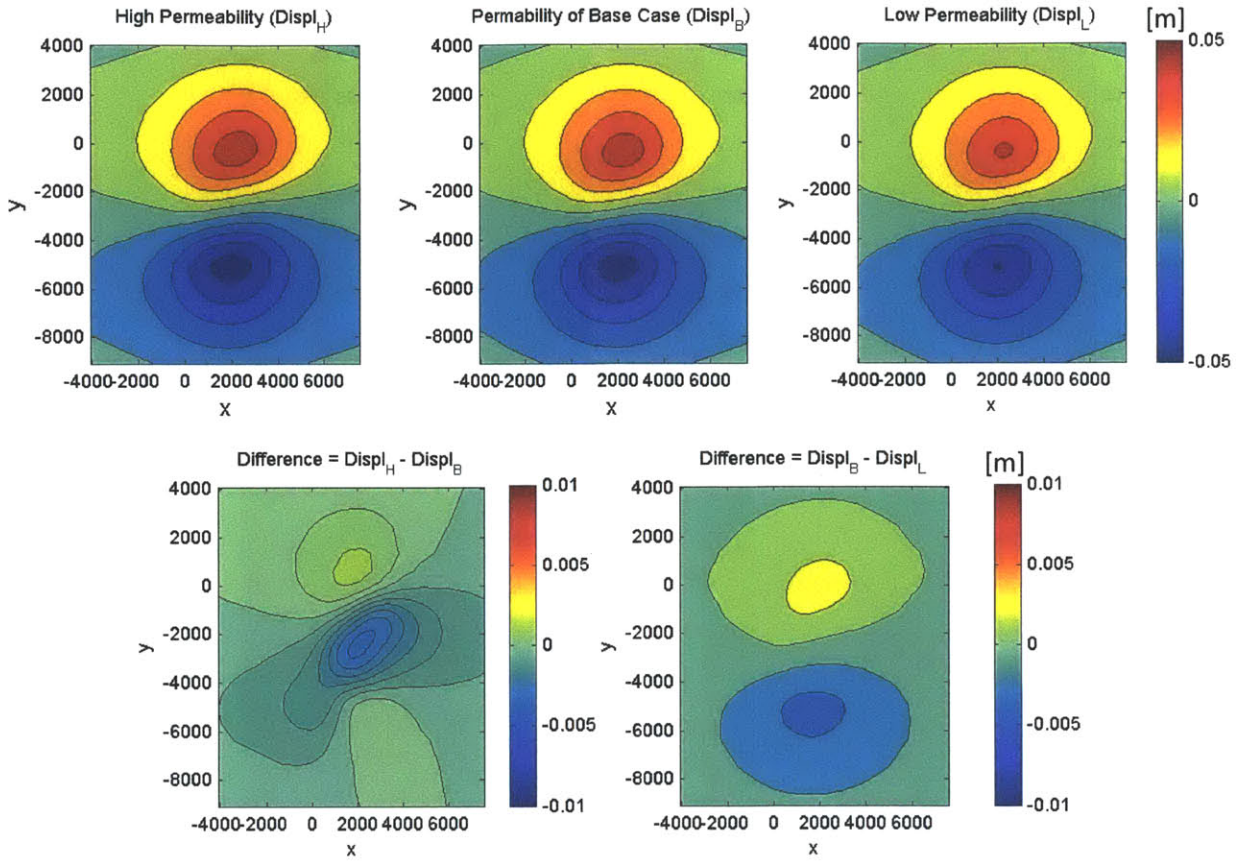

Figure 39 Comparison of the displacement fields [m] in the y-direction on January 1, 1976 when the permeability in all directions is multiplied by 1.2 times (i.e., high permeability) and is 80% of that of the base case (i.e., low permeability)

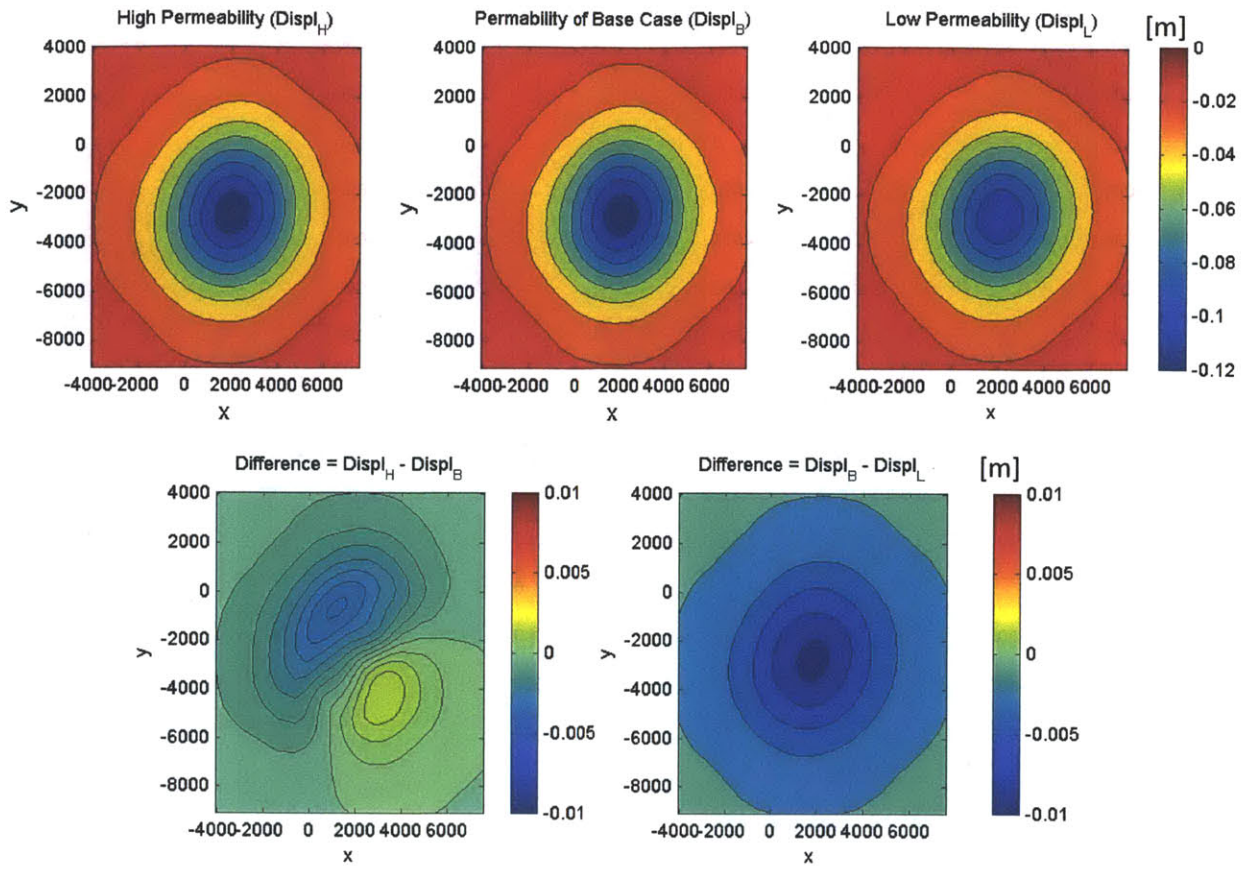

Figure 40 Comparison of the displacement fields [m] in the z-direction on January 1, 1976 when the permeability in all directions is multiplied by 1.2 times (i.e., high permeability) and is 80% of that of the base case (i.e., low permeability)

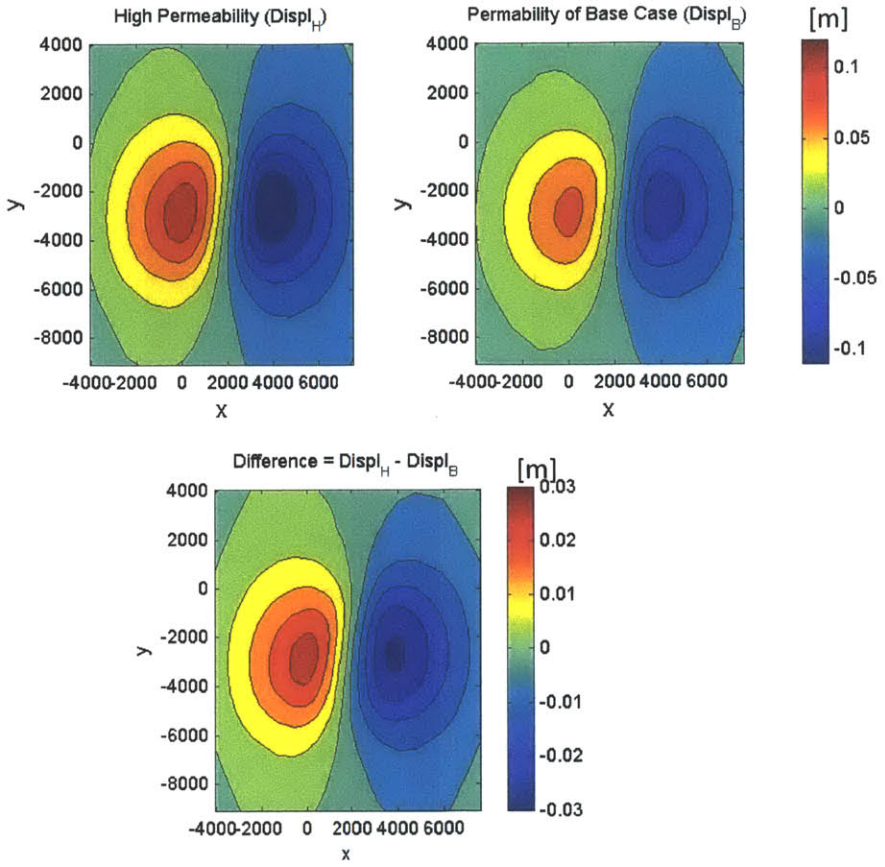

Figure 41 Comparison of the displacement fields [m] in the x-direction on July 1, 1983 with the nominal case when the permeability in all directions is multiplied by 10 times (i.e., high permeability).

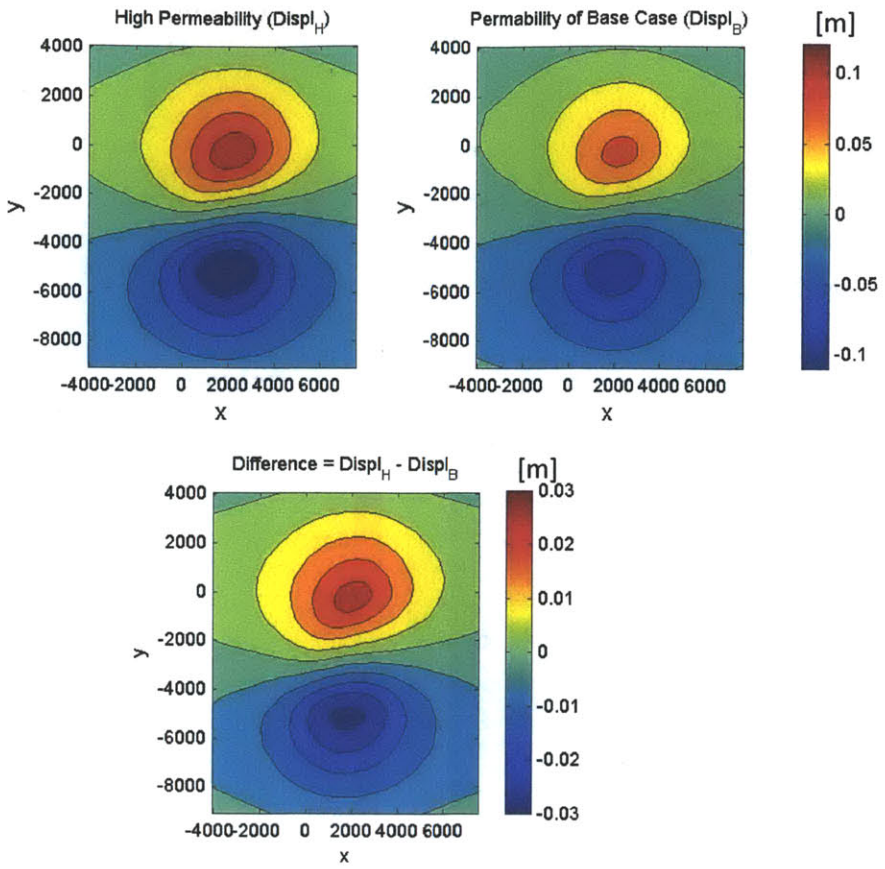

Figure 42 Comparison of the displacement fields [m] in the y-direction on July 1, 1983 with the nominal case when the permeability in all directions is multiplied by 10 times (i.e., high permeability).

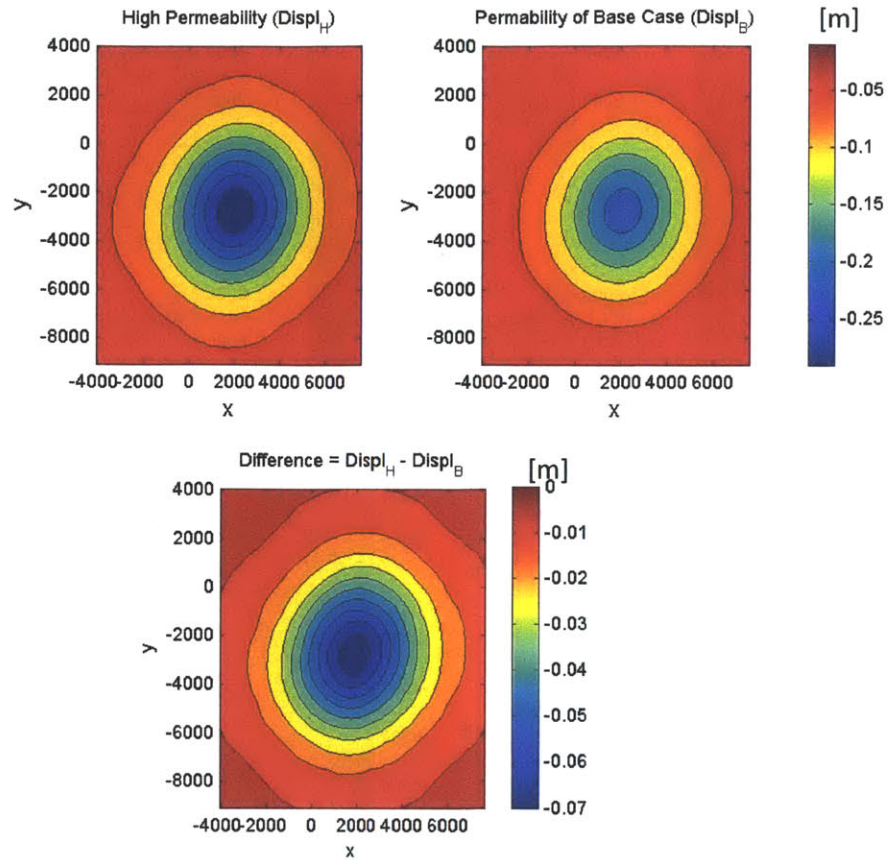

Figure 43 Comparison of the displacement fields [m] in the z-direction on July 1, 1983 with the nominal case when the permeability in all directions is multiplied by 10 times (i.e., high permeability).

Sensitivity to Young's Modulus

As long as the production rates of the field are the same in any cases, the surface deforms less with a lower Young's Modulus (higher porosity) and deforms more with a higher Young's modulus (lower porosity). However, the changes are not drastic. Figure 44 to Figure 46 show the results when the porosity is increased and decreased by 20%.

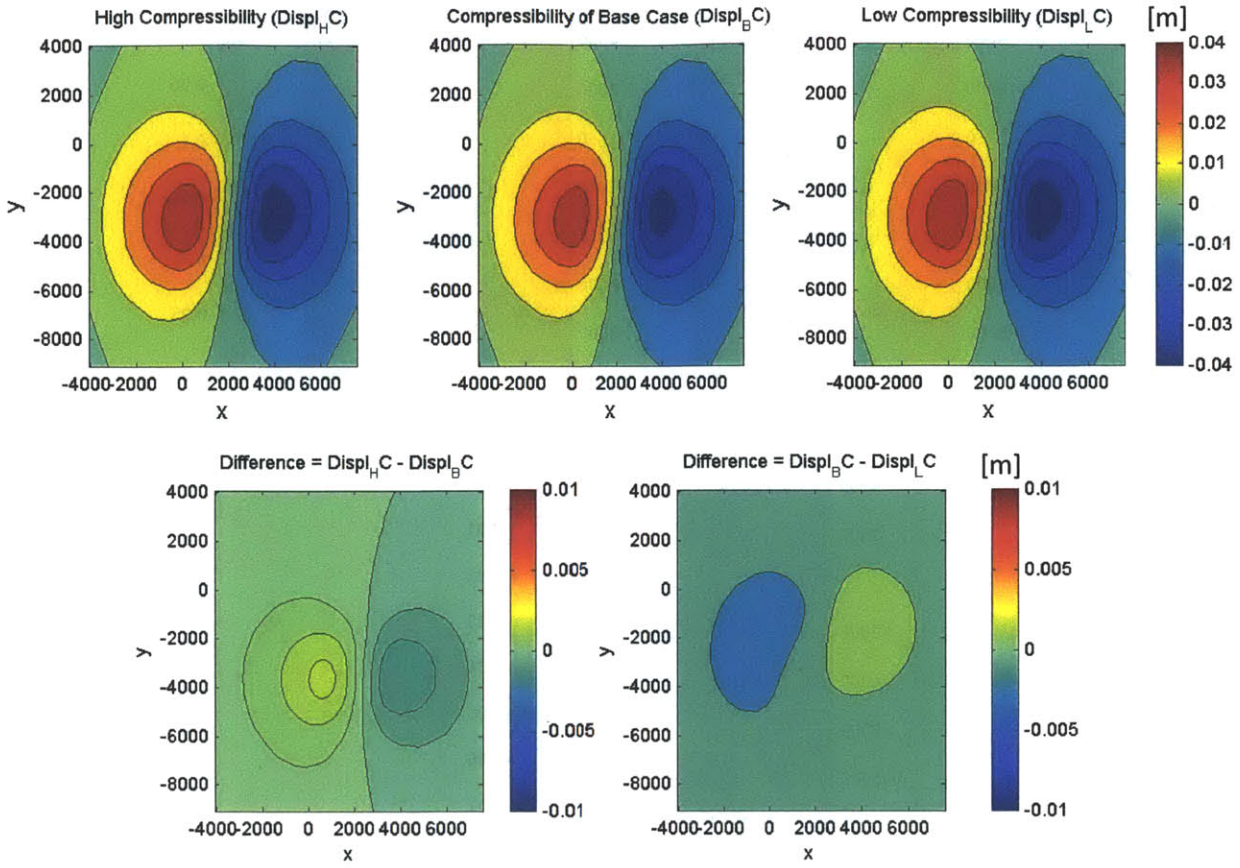

Figure 44Comparison of the displacement fields [m] in the x-direction when the porosity is increased by 20% (i.e., high compressibility) and decreased by 20% (i.e., low compressibility) of the nominal case.

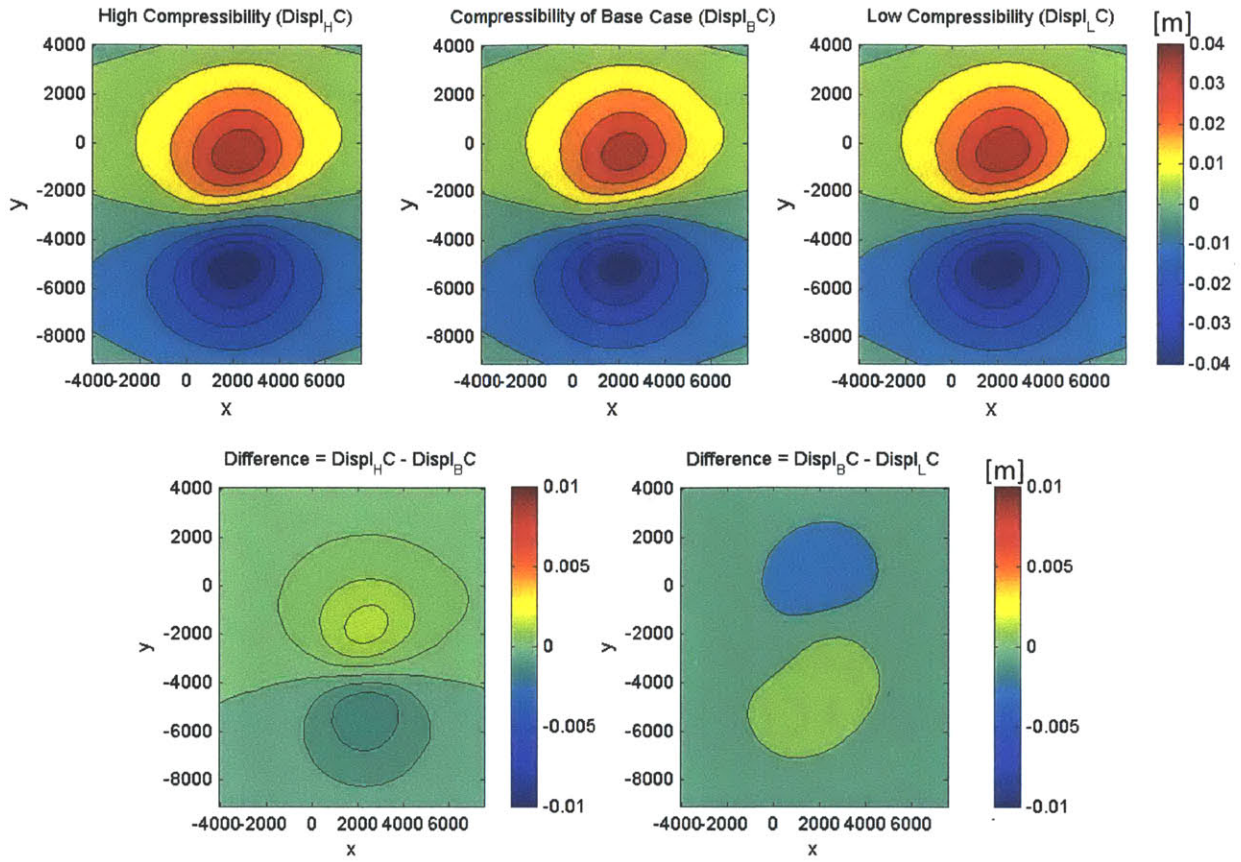

Figure 45Comparison of the displacement fields [m] in the y-direction when the porosity is increased by 20% (i.e., high compressibility) and decreased by 20% (i.e., low compressibility) of the nominal case.

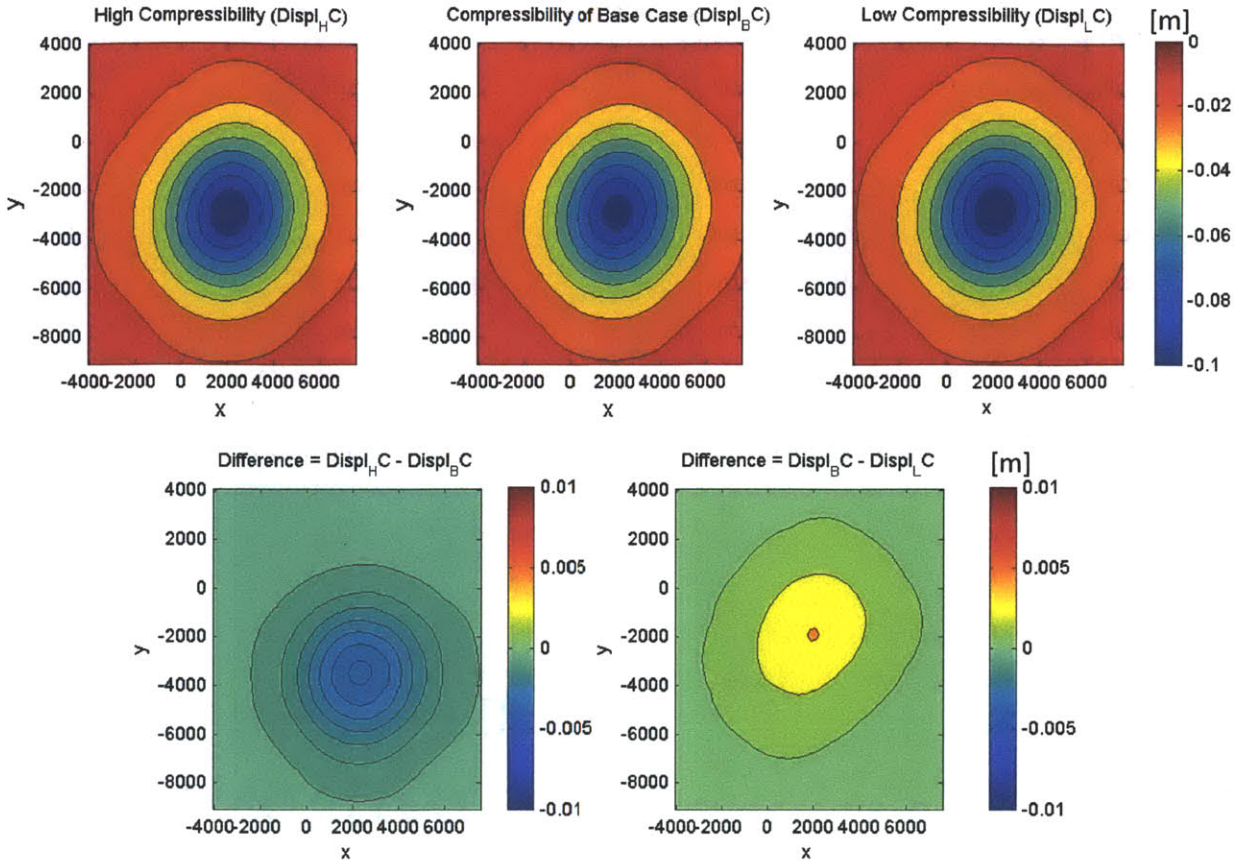

Figure 46 Comparison of the displacement fields [m] in the z-direction when the porosity is increased by 20% (i.e., high compressibility) and decreased by 20% (i.e., low compressibility) of the nominal case.

Sensitivity to the Depth of the Ground Surface

We are interested to see if a lower ground level would affect the surface displacement drastically. Figure 47 to Figure 49 show that the ground does deform much more if the reservoir is situated closer (~ 1350 to 1400 m) to the ground.

This may be due to the fact that there are less thick of an overburden layer above the reservoir. Whenever wells are pumped, the reservoir layer is compressed. This normally stretches the layers of rock above the reservoir. As we limit the thickness of the overburden, this compression is compensated less by extending a less thick of an overburden. As the ground is closer to the reservoir underground, any downward displacement of the reservoir is more easily felt on the ground surface.

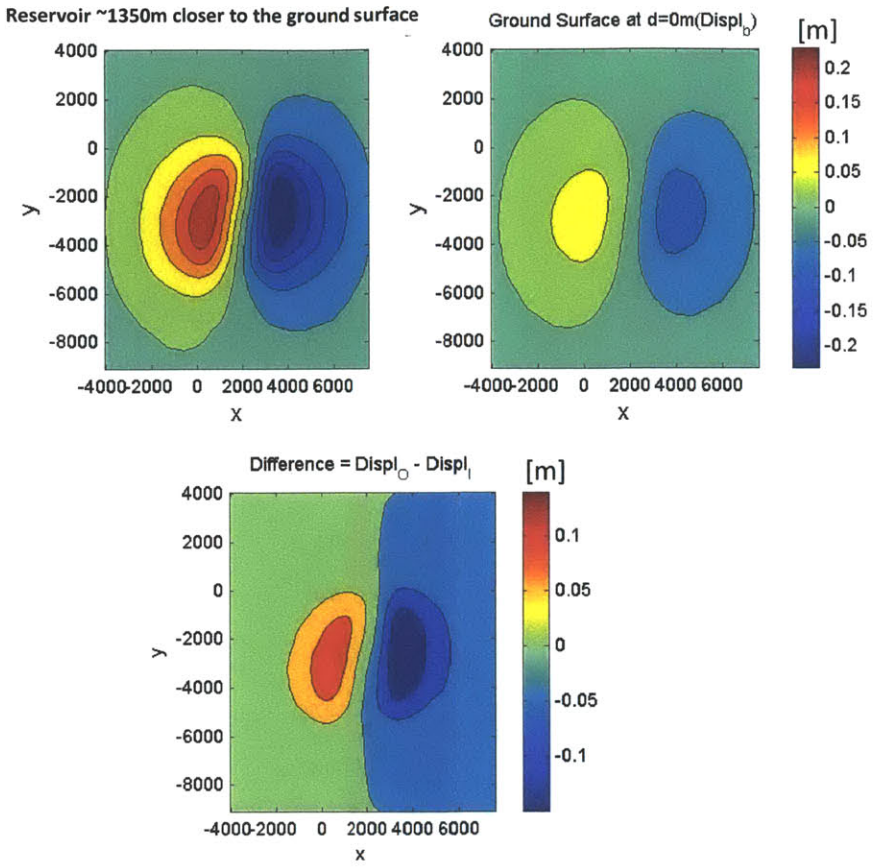

Figure 47Comparison of the displacement fields [m] in the x-direction when the reservoir is ~1350m closer to the ground surface

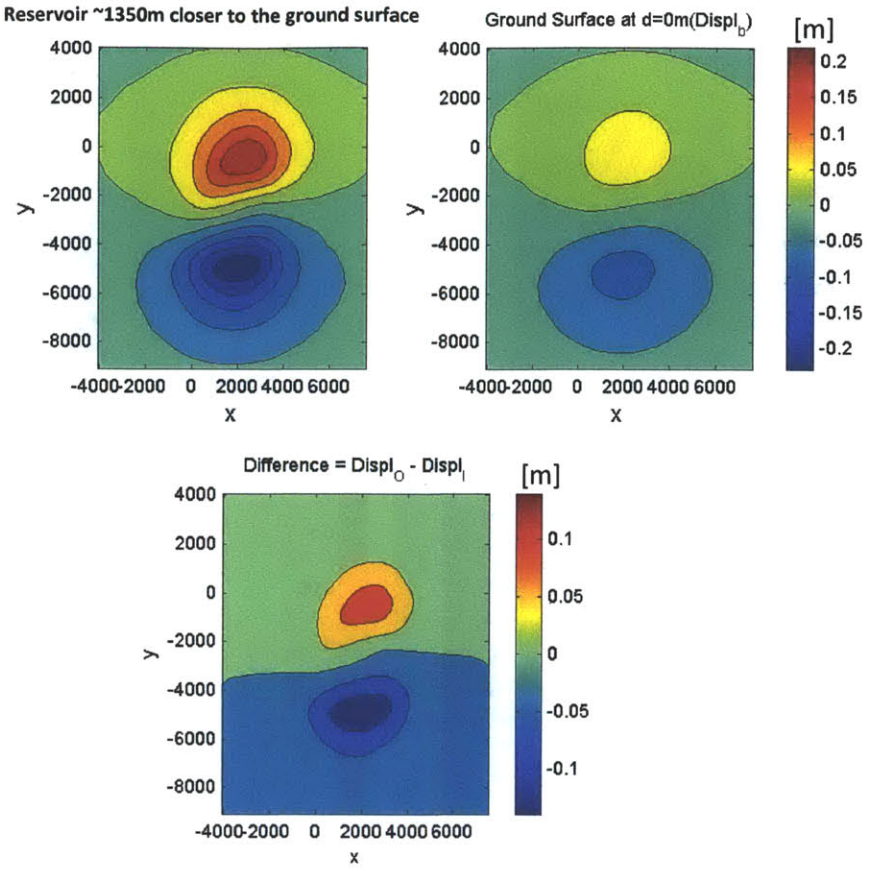

Figure 48Comparison of the displacement fields [m] in the y-direction when the reservoir is ~1350m closer to the ground surface

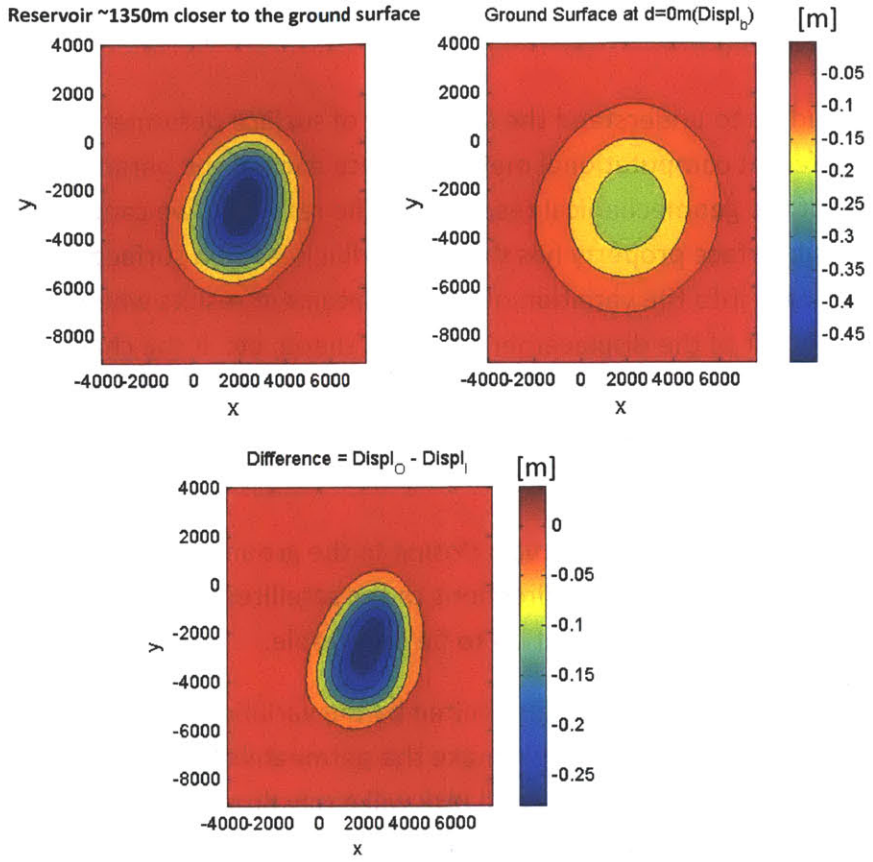

Figure 49Comparison of the displacement fields [m] in the z-direction when the reservoir is ~1350m closer to the ground surface.

Chapter 7 - Conclusion

Our goal in this study is to understand the sensitivity of surface deformation to subsurface properties and different computational methods. Since each of the parameters governs different aspects of the geomechanical response of the reservoir, we cannot simply conclude which particular subsurface property has the most influence upon surface deformation. Rather, we should look into the variation of the displacement results when each parameter is adjusted: the contour of the displacement field, its shape, etc. If the change of displacement is big enough to be detected by INSAR or GPS (detectable and accurate within millimeter scale), we can estimate the subsurface properties of the reservoir with more accuracy.

Among the four tests, moving the reservoir closing to the ground surface easily yields more signal of the surface subsidence in all directions to the satellites. The deeper the reservoir is, the harder it is for the surface deformation to be detectable.

As for other tests, our sensitivity tests are limited by the variation of the compressibility and the permeability that we can adjust. If we make the permeability too low or the compressibility too high or too low, the well BHP will easily drop below the minimum allowable level. Technically we can accommodate this by lowering the minimum well BHP allowed in the simulation. However, we will still like to keep the minimum well BHP at a reasonable yet realistic level, just like in any day-to-day reservoir operations. Therefore, we rather change the permeability and compressibility slightly (by only increasing or decreasing 20% from the base case parameters), trying to see if the change in the surface deformation is significant enough to be detected by INSAR or GPS.

Indeed for the compressibility test, the difference in the z-direction displacement can be better captured by INSAR than the lateral displacement in the x- and y-directions (10 mm of maximum difference in the vertical direction as supposed to 1 mm of maximum different in the lateral directions). But all these changes in the displacements agree with the theoretical equations qualitatively, be the quantitative differences large enough or too small to be detected.

For the permeability test, increasing the permeabilities in all directions by 20% does not make the changes of any displacement results as detectable as that when the permeabilities reduced by 20%. When the permeabilities are increased by 20%, the displacement differences in any directions are rather obscured in terms of qualitative signals even (Figures 38 to 40). This is partly because we compare the results at an earlier time of the simulation.

Thus we try to increase the permeabilities by 10 times instead and compare the results at the end of the simulation. Both qualitatively and quantitatively, the differences show no such an issue as before and they are much more apparent to be captured by INSAR or GPS.

It is believed that iterative coupling computes deformation more accurately than one-way coupling. The displacement results of iterative coupling in the z-direction, being about 3mm to 6mm deeper than the one-way coupling results in the area of major focus (that is, right around where the reservoir situates), are definitely detectable by INSAR.

However, there is a discrepancy between the displacement results from STARS and Abaqus as a result of one-way coupling computation. The difference between the two displacement fields in the z-direction can go as high as 19mm at the point of highest vertical displacement (close to the center of the field, where the reservoir situates). Even laterally, the differences can go as high as 12 mm to 20 mm in the x- and y-directions respectively. This difference is of our concern, as there is no need to add errors to these forward models of which discrepancy of the results will be detectable by satellites. This can be attributed to the fact that we adopted a different mesh for the finite element computation on geomechanics. In STARS, we apply two meshes, finite volume mesh for fluid flow calculation and finite element mesh for geomechanics calculation. These 2 grids are set up differently in Abaqus. That means the fluid flow and geomechanics calculations are connected differently in one-way coupling computation. Also, different well models are used in STARS and in ECLIPSE.

Nevertheless, the discrepancy would complicate the surface deflection measurements which will be fed into the EnKF for inversions on the PUNQ sample problem. As we would like to predict the subsurface properties and surface deformation accurately, this issue needs to be resolved with further studies.

As the next step, we would like to implement the Ensemble Kalman Filter (EnKF) on PUNQ. EnKF will be used to characterize the subsurface properties of the reservoir and to forecast the surface deformation under various production scenarios. Since no surface deformation data of PUNQ is available, we hope to apply EnKF on an actual gas reservoir with historical INSAR and GPS data recording the ground surface movement during operation.

Bibliography

Chang, Haibin, Yan Chen and Dongxiao Zhang. "Data Assimilation of Coupled Fluid Flow and Geomechanics Using the Ensemble Kalman Filter." SPE Resevoir Simulation Symposium. Texas: Society of Petroleum Engineers, 2009.

Chen, Zhangxin, Guanren Huan and Yuanle Ma. Computational Methods for Multiphase Flows in Porous Media. Society of Industrial and Applied Math (SIAM), 2006.

Computer Modeling Group Ltd. "User's Guide: STARS, Advanced Process and Thermal Reservoir Simulator." 2011.

Geertsma, J. "The Effect of Fluid Pressure Decline on Volumetric Changes of Porous Rocks." Petroleum Transactions, AIME, Volume 210 (1957): pages 331-340.

Imperial College. Imperial College London. <http://www3.imperial.ac.uk/earthscienceandengineering/research/perm/punq-s3model>.

Terzaghi, Karl von. Theoretical Soil Mechanics. New York: J. Wiley and Sons, inc., 1943.

Tran, David, Long Nghiem and Lloyd Buchanan. "Aspect of Coupling Between Petroleum Reservoir Flow and Geomechanics." 43rd US Rock Mechanics Symposium and 4th US-Canada Rock Mechanics Symposium. Asheville, NC, 2009.

Vasco, Donald W. "A Coupled Inversion of Pressure and Surface Displacement." Water Resources Res. (2001).